PONTIFICIA UNIVERSIDAD CATOLICA DE CHILE
ESCUELA DE INGENIERIA

NUMERICAL MODELLING OF THE CYCLIC TORSIONAL SHEAR TEST ON GRANULAR MEDIA

J.F. WILSON

Thesis submitted to the Office of Research and Graduate Studies in partial fulfillment of the requirements for the Degree of Master of Science in Engineering

Advisor:
ESTEBAN SÁEZ

Santiago de Chile, August 2016

PONTIFICIA UNIVERSIDAD CATOLICA DE CHILE
ESCUELA DE INGENIERIA

NUMERICAL MODELLING OF THE CYCLIC TORSIONAL SHEAR TEST ON GRANULAR MEDIA

JOSÉ FRANCISCO WILSON COLLAO

Members of the Committee:

ESTEBAN SÁEZ ROBERT

CARLOS OVALLE ORTEGA

JUAN CARLOS QUEZADA GUAJARDO

JOSÉ RICARDO PÉREZ CORREA

Thesis submitted to the Office of Research and Graduate Studies in partial fulfillment of the requirements for the Degree of Master of Science in Engineering

Santiago de Chile, August 2016

Gratefully to my family

ACKNOWLEDGEMENTS

I am deeply grateful to everyone who made this research possible and supported me in this process, which has been immensely important for my personal and professional development. To Javier Camacho, for his work and valuable help in the implementation process of the Resonant Column Apparatus. To Antonio Salazar, for his great willingness to share his work, ideas and knowledge from previous research on DEM. To Carlos Ovalle, for his support and concern in the first stage of laboratory tests and material characterization. To Guillermo Poblete, for his constant support and valuable assistance at the laboratory.

I am especially grateful to my supervisor Esteban Sáez, who has been an exceptional mentor, encouraging me and strengthening my skills. Furthermore, I want to thank the time, patience and effort for teaching me and guiding me to achieve this academic work. I also want to thank the given opportunity and the flexibility for allowing me to follow my own projects during this process.

TABLE OF CONTENTS

LIST OF FIGURES

LIST OF TABLES

ABSTRACT

In this research, a torsional cyclic shear test was modeled using the 3D discrete element method (DEM). The results are compared against experimental data and micromechanical aspects of the tested material during the loading are discussed. The focus of the investigation is to study the homogeneity of strains during this laboratory test, and to compare the micro-mechanical behavior of the granular media for different strain levels.

The experimental investigation was performed using a synthetic material made of glass beads, which simplifies the modelling and calibration since normal interaction forces does not induce rotation of the particles. A uniform and a non-uniform particle size distribution have been studied to assess the role of particles packing on the experimental results and its modeling by DEM.

Calibration stage consisted in an adjustment of particle's contact fiction using a DEM model of the direct shear test based in the work of Salazar et al. (2015). After that, it was developed the torsional shear test model using the material properties calibrated in the previous step. Both models and experimental tests used the same grading distribution and particle size.

We showed that the model of the torsional shear test can properly reproduce the hysteresis cycles in terms of shape and magnitude. Thus, it was obtained a robust estimation for the secant shear modulus and damping ratio at different strain level. With this, it was possible to build a stiffness degradation and damping increase curve and compare with experimental data obtained from torsional shear tests. Based on this validation model, it is discussed the stress and strain behavior of the granular material and its relation with the macroscopic parameters obtained. It is shown that shear strain distribution on the sample becomes relatively larger close to the top of the sample as top rotation increases, i.e. different to standard assumption of uniform strain distribution.

Keywords: DEM, Torsional shear test, cyclic loading, shear modulus, damping ratio, micro-parameters, degradation curve, granular media.

RESUMEN

En esta investigación fue modelado un ensayo de corte cíclico de torsión utilizando el método de los elementos discretos 3D (DEM). Los resultados se comparan frente a datos experimentales y se discuten los aspectos micro-mecánicos del suelo durante el ensayo. En particular, el énfasis de la investigación es estudiar la homogeneidad de las deformaciones durante esta prueba de laboratorio, y comparar el comportamiento micro-mecánico de la muestra de suelo para diferentes niveles de deformación.

La investigación experimental se realizó con un material sintético de esferas de vidrio que simula un suelo, lo que simplifica el modelamiento y la calibración ya que las fuerzas de interacción normales no inducen rotación de las partículas. Se estudió una granulometría uniforme y otra no uniforme para evaluar el rol de la granulometría del suelo en los resultados experimentales y su modelación mediante DEM. La etapa de calibración consistió en un ajuste de la fricción de contacto de partículas usando un modelo DEM del ensayo de corte directo basado en el trabajo de Salazar et al. (2015). A continuación, se desarrolló el modelo de ensayo de corte torsional utilizando las propiedades del material calibrado en el paso anterior. Ambos modelos y pruebas experimentales utilizaron la misma granulometría y tamaños de partícula.

En este estudio se demuestra que el modelo del ensayo de torsión puede reproducir correctamente los ciclos de histéresis tanto en inclinación como amplitud. Por lo tanto, se obtuvo una estimación robusta para el módulo de corte secante y factor de amortiguamiento en diferentes niveles de distorsión angular. Con esto, fue posible construir una curva de degradación de la rigidez y de aumento de amortiguamiento y comparar con los datos experimentales obtenidos a partir de ensayos de torsión cíclica. Se muestra que la distribución de tensiones y deformaciones en la muestra se concentran cerca de la parte superior a medida que aumenta la amplitud del giro, es decir, distinto al supuesto estándar de distribución de deformación uniforme.

Palabras Clave: DEM**,** ensayo de torsión cíclica, carga cíclica, módulo de corte, amortiguamiento, micro-parámetros, curva de degradación, medio granular sintético.

1. INTRODUCTION

1.1 Motivation

The dynamic properties of soils are widely studied parameters due to its importance to analyze and design geotechnical structures subjected to external dynamic loadings such as vibrations or earthquakes. These loads vary depending on frequency, amplitude, loading rate and the repetition or number of cycles (Ishihara 1996), which generates degradation on the stiffness of the material, as well as an increase of damping. Several laboratory studies have tried to simulate *in-situ* conditions to study this behavior.

To solve most of soil dynamic problems it is required to determine parameters which allow characterizing the dynamic behavior of soils (Shear modulus and Damping ratio). One of the laboratory methods used to obtain dynamic parameters of soils is the cyclic torsional shear test. This test is commonly used to investigate the dynamic behavior of soils under isotropic or anisotropic initial stress conditions. Imposing a cyclic shear stress on horizontal planes it is possible to measure stiffness and damping characteristics over a wide range of strain levels (Kramer, 1996). During the test, it is possible to consider different frequencies, amplitudes and number of cycles of loading. Despite the great amount of experimental data, it is not possible yet to have a well knowledge of the micro-mechanical behavior of soil during cyclic loading. Because of this, it is imperative to use the computational and numerical tools to solve this problem.

In 1979, Cundall & Strack introduced the Discrete Element Method (DEM). This method is a discontinuous numerical method which models the soils as a group of individual particles calculating the movement and forces due the mechanical interactions between them. This methodology allows having a control of the position and interaction forces of the whole medium, allowing performing a micro-mechanical analysis of the material, which represents a limitation of the real test in laboratory. With this and other qualities of the DEM methodology, it is aimed to reproduce the Torsional shear test from experimental data in order to study micro-mechanical aspects of granular soils.

1.2 Objectives and methodology

The main goal of this investigation is to explore micro-mechanical aspects of the experimental cyclic behavior of granular materials. With this purpose in mind, this work was separated in two parts.

Laboratory stage:

- Perform Torsional Shear and Resonant Column tests of two different grading curves at different confinement pressures using a synthetic granular material made of glass beads.
- Using the laboratory results, obtain the hysteresis and degradation curves which will be used to compare and to calibrate the DEM model.

Numerical modeling stage:

- Be able to reproduce through DEM the response of a glass-beads sample which is submitted to a Torsional Shear test.
- Study micro-mechanical aspects of the particle's behavior and the relation of the micro-mechanical parameters with the macroscopic dynamic parameters of the material such as Shear modulus and material Damping.

In order to explore the micro-mechanical behavior of granular materials in the Cyclic Torsional Shear test, two different grading curves of glass beads were chosen. There were made multiple specimens to be tested at different confinements.

Several test of the Torsional Shear test and Resonant Column test were performed in order to compare the results and study the degradation curves at different amplitudes and frequencies.

Once the laboratory stage is done, the Torsional Shear Test was modeled numerically through DEM. The friction of the model was calibrated initially using direct shear tests and the corresponding DEM model from Salazar et al (2015).The rest of the parameters were calibrated using experimental data of the Torsional Shear test, aiming to replicate the hysteresis cycles obtained in laboratory and evaluating the ability of the model to replicate the real test and then studying the relative movement and interaction between particles and its relation with the observed inelastic macroscopic behavior.

1.3 Description of a granular material

To start with, it is important to describe the nature of the tested material. A particulate media is very different from solids, liquids or gas. A Granular material is defined as an assembly of discrete solid particles interacting with each other due to dissipative collisions. Several types of granular materials are present in nature, like sand or snow, but they can also be found in the industry with the shape of powders, chemicals or groups of products that are processed together. The mechanical behavior of this material depend on force interactions between particles, defining the mechanics of granular flows.

Since a granular system is composed of individual particles and each particle moves independently of each other, it is difficult and computationally expensive to predict the behavior of granular system using continuous models. Nowadays the computational power has increased and the computer's processors are able to solve problems related with granular media .This kind of simulations are carried out to understand the behavior of this materials in many engineering fields and day after day they are becoming more important and taken into account for scientists and engineering design.

In this context, the discrete approach developed for particle scale numerical modelling of granular materials has become a powerful and reliable tool. This approach is called as Discrete Element Method (DEM), it is considered as an alternate to the continuum approach. The philosophy behind the DEM simulation is to model the system at microscopic level or particle level and study their behavior including the detection of contacts and interaction between particles and their environment. DEM can efficiently and effectively model the dynamics of assemblages of particles. Technically, the discrete approach requires a time-discretized form of equations of motion governing particle displacements and rotations, and a force law or force-displacement relation describing particle interactions. DEM is particularly useful in modelling materials that undergo discontinuous deformations because of the contact with other particles in the system, breakage of contact bonds and compaction of broken fragments.

Although the motion of the particles is resolved with DEM, the interaction with fluid flows is not directly captured. Nevertheless, some methodologies to adding and analyze

the fluid flow behavior exists, for instance the computational fluid dynamic (CFD) method. In this approach, the flow of continuum fluid is described by Navier-Stokes equations, then the granular phase occupies a certain volume in each computational cell and it is accounted for by introducing a "volume fraction" into the fluid dynamics equations. Furthermore, the granular and fluid phase can exchange momentum, heat and mass (CFDEM.com, 2016). Others extensions to take into account the capillary effects solving the Laplace-Young equation are available. This equation relates the pressure difference to the shape of the spherical elements, which represents the interaction as a result of capillary bridges between each pair of particles.

Particularly, in this investigation CDF coupling is not used since this research aims to simulate a granular media in dry condition, subjected to cyclic loads simulating an earthquake as drained loading.

2. TORSIONAL SHEAR TEST

2.1 Overview

The torsional shear test is a commonly used laboratory test for measuring the dynamic soil properties at low to medium strains (i.e. 10^{-4} to 10^{-2} %). The aim of Torsional shear test is to determine shear modulus and damping properties of either solid or hollow cylindrical soil specimens. This test is performed under saturated conditions, so that the specimen is subjected to a saturation and consolidation stage.

This testing technique consist in a cylindrical sample fixed at the base subjected to a cyclic torsional force. The torsional excitation on the top is applied through a rigid mass exited by an electromagnetic loading system (Fig 1a.). This test is performed at a sinusoidal varying amplitude torque at a fixed frequency, which means that it is a force-controlled test. Hence, the effective angular deformation due the torsional loading will depend on the stiffness and confinement of the sample.

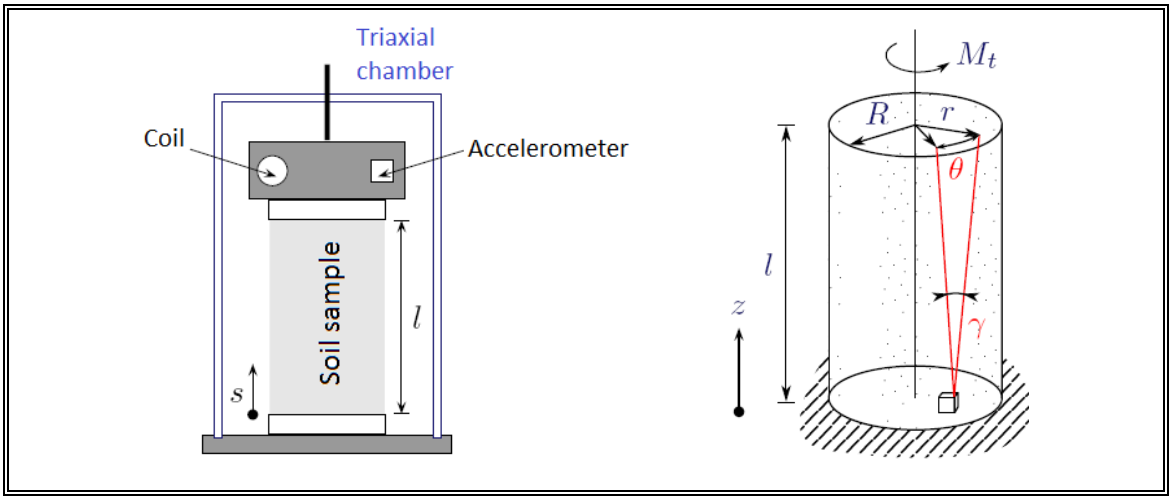

Figure 2.1: Schematic representation of Torsional Shear Test (TS) (modified from Sáez, 2016)

In contrast to resonant column tests, torsional shear tests are conducted at frequencies below 2Hz. In these tests, the dynamic response of the specimen is evaluated

using shear stress-strain curves, referred to as hysteresis loops. From these curves, the shear modulus and hysteretic damping ratio can be determined as it is explained later.

2.2 Shearing stress-strain

Shearing stress, shown in Eq. (2.1) is calculated using theory of elasticity applied to a cylindrical bar in pure torsion. Where R and J_p are the current radius and polar moment of inertia of the specimen and T is the applied torque.

$$\tau = \frac{RT}{J_p} \qquad (2.1)$$

The applied torque calculation is shown in Eq. (2.2). This value is calculated from the output current from the torsional drive system (A_T) and the torque output calibration factor (C_T). For the equipment used in this study, the mentioned constant has a value of 0.4758 [Nm/A].

$$T = A_T C_T \qquad (2.2)$$

The shearing strain can be easily measured using the twist angle (θ) shown in Eq. (2.3) and the given outputs from the experimental device. As the Torque calculation, the twist angle comes from an output measured in voltage from the torsional drive system (O_s) multiplied by a strain output calibration factor (C_s) which has a value of 3.36 [mrad/V].

$$\theta = O_s C_s \qquad (2.3)$$

Finally, the shear strain may be calculated from Eq. (2.4), where l is the specimen height.

$$\gamma = \theta \frac{r}{l} \qquad (2.4)$$

The shearing strain amplitude varies across the radius of the specimen from a cero value from along the central axis of rotation. It is suggested to use 0.8 times the radius ($r = 0.8R$) in order to have a presentative shear strain for a given specimen. Fig.1 shows that the value of angular distortion is constant in the height of the specimen, this can only state strictly in elastic range. Then, the focus of the research will be study the distribution of this distortion through the height of the specimen to corroborate the usual hypothesis of strain homogeneity.

2.3 Shear modulus

In the torsional shear test the Shear modulus corresponds to the slope of the hysteresis loop, calculated from Eq. (2.5). The shearing stress (τ_{pp}) and shear strain(γ_{pp}) are considered from peak to peak values of the hysteresis loop (Figure 2.2).

$$G = \frac{\tau_{pp}}{\gamma_{pp}} \qquad (2.5)$$

2.4 Damping ratio

The value of damping represents the energy dissipation due frictional relative displacements in dynamic problems involving granular materials. The amount of dissipated energy during one loading cycle and the peak strain energy in the specimen during this cycle are used to calculate the hysteretic damping ratio. The dissipated energy can be measured by determining the area of the hysteresis loop (A_l). While the peak strain energy is measured by finding the area under the secant modulus line from cero to peak strain value (A_t). Thus, the hysteretic damping ratio, λ is shown in Eq. (2.6).

$$\lambda = \frac{A_l}{4\pi A_t} \qquad (2.6)$$

The shape of the hysteresis loop can be approximated to an ellipse. The area of the ellipse (A_e) can be calculated from Eq. (2.7) where L and $B$are the length and width of the ellipse.

$$A_e = \frac{\pi}{4} LB \qquad (2.7)$$

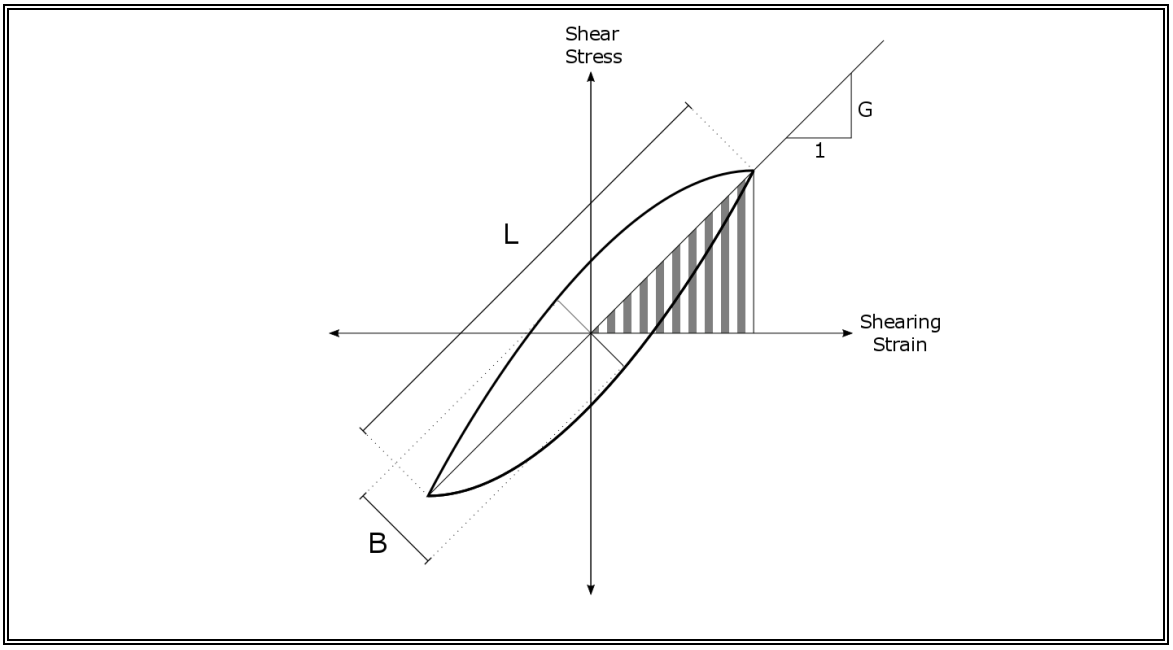

Figure 2.2: generic hysteresis loop from TS test

2.5 Torsional Shear device

2.5.1 Equipment description

The Resonant Column/Torsional Shear apparatus used in this investigation corresponds to a CONTROLS® combined device for the automatic determination of shear modulus and damping ratio. These parameters can be calculated either from half power bandwidth and free vibration decay in the case of Resonant Column and hysteresis loop

in the case of Torsional Shear test (Figure 2.3). This system is supplied with a triaxial chamber made of an acrylic transparent cylinder with 170 mm diameter and 15 mm thickness. For applying confinement to the sample it is used a mixed air/water chamber both communicated from the top, the inner chamber is filled with water and the outer chamber applies the confinement pressure using compressed air. This system is able to resist up to 1000 kPa pressure.

An electrodynamics floating frame drive system is used to apply torque to the specimen. The drive system consists of a drive plate, drive coils, a power current amplifier. The internal data acquisition system generates all the signals necessary to drive the torque motor. The drive plate is the four-armed plate armed with NeFeB magnets attached to the end of each arm. Eight drive coils encircle the end of each magnet. The drive late and coils constitute an electric motor to apply torque on the specimen using a sinusoidal current. The coils are wired together so the drive plate acts in pure torsion. Each coil is shaped so that the magnets may move inside the coil as the specimen shortens or bends during the consolidation. The frequency and DC offset to torsional drive system is provided by the data acquisition and the control board located into the main control board (controls-group.com, 2013).

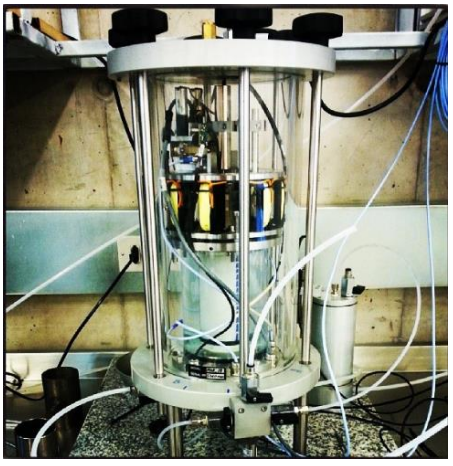

Figure 2.3: CONTROLS® device used to conduct TS tests

This system also includes a sensor kit with axial, volumetric and pressure transducers, current displacement sensors and MEMS accelerometers. PC and software are provided for continuously monitoring and recording all parameters and performing the test both automatically or manually.

This device is able to perform tests up to 10 degrees maximum angular deformation and at 1.2 Nm maximum torque. The cyclic excitation frequency for TS test goes from 0 to 50 Hz and the dynamic excitation frequency for RC test goes from 1 to 300 Hz.

2.5.2 Experimental setup example

In this case, the tested sample is prepared on the equipment's base. First, the membrane is fixed to the base (porous stone) by rubber rings, then the mold is assembled and filled with the synthetic material. Finally, it is installed the clump head and fixed to the membrane with rubber rings as it is shown in the Figure 2.4.

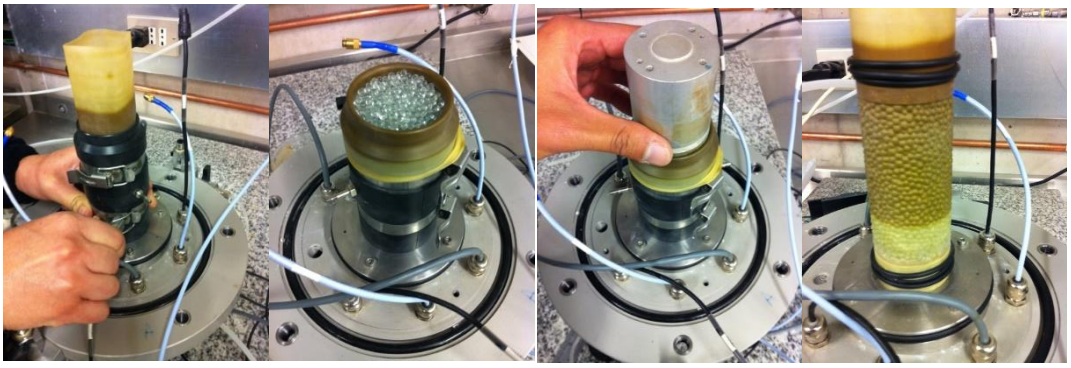

Figure 2.4: example of sample preparation in the device

Because it is a cohesionless remolded sample, it is necessary to apply vacuum to confine the sample and ensure that maintain the shape it was given with the mold. The vacuum is applied through a backpressure valve, ensuring that the valve connecting the cylinder volume control with the sample is closed.

After the sample is in position, the device has to be assembled. First, the water chamber is installed and the electrodynamic frame with magnets is fixed at the top. The magnets must be well centered within the coils and without bumping the base. Special care is taken when entering the head metal tools as it can damage the magnets.

Then, the shift plates are fixed to the head of the specimen and the movement transducer is installed (proximeters) at a suitable height in order to ensure a full contact with the plates described previously.

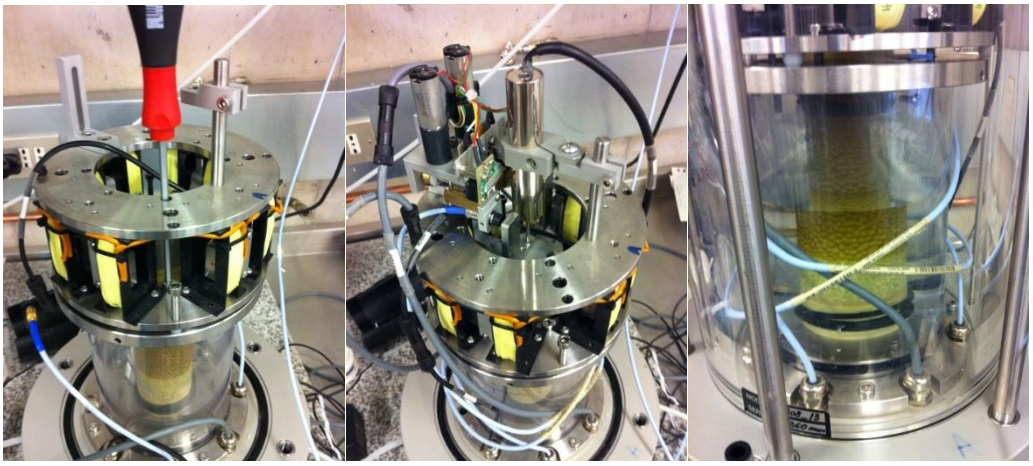

Figure 2.5: example of assembling of the double chamber and torsional actuator

The next step is to connect the wires. There are 6 wires, *Prox1*, *next2*, *Accel*, *Coils* and *Axial*. The coil wire is connected to the base of the top of the unit, the motion cable attaches to the motion transducer, accelerometer wire is connected to the top of the unit (magnets), and the axial cable is connected from the transducer to the axial cable from the computer base. Finally proximeter wires goes from motion transducer to the base, both labeled.

2.6 Experimental results

The experimental work focused on the investigation of the mechanical behavior of the synthetic granular material through resonant column and cyclic torsional shear tests. First, a poorly graded sample (G1) of glass beads was used for the tests, a 100% of the grains are bigger than 2.65 mm diameter and were retained in sieve #8 (2.35 mm). Then, it is tested a non-uniform sample (G2) with grains distributed in sieves #8, #16 and #30 being retained a 0.65, 0.31 and 0.085 percent of the total weight respectively. The smallest sieve retains all the grains above 0.6 mm. The material has a specific gravity (G_s) equal to 2.51 and a maximum and minimum void ratios 0.69 and 0.61 respectively. All the tests were performed using samples with 40% of relative density.

2.6.1 Resonant Column tests

Cyclic loading was applied to the uniform specimen for 10 to 20 s recording using a frequency step of 1 Hz. During this period, loading cycles were applied at resonant frequencies ranged from 80 Hz to 160 Hz for strain measurements at 100 kPa effective stress and from 100 to 180 Hz for a sample confined with 200 kPa pressure.

The tests were performed at amplitudes varying from 0.0005V to 0.5V, which represents a range of strain starting from 10^{-4} to 2×10^{-2} %.

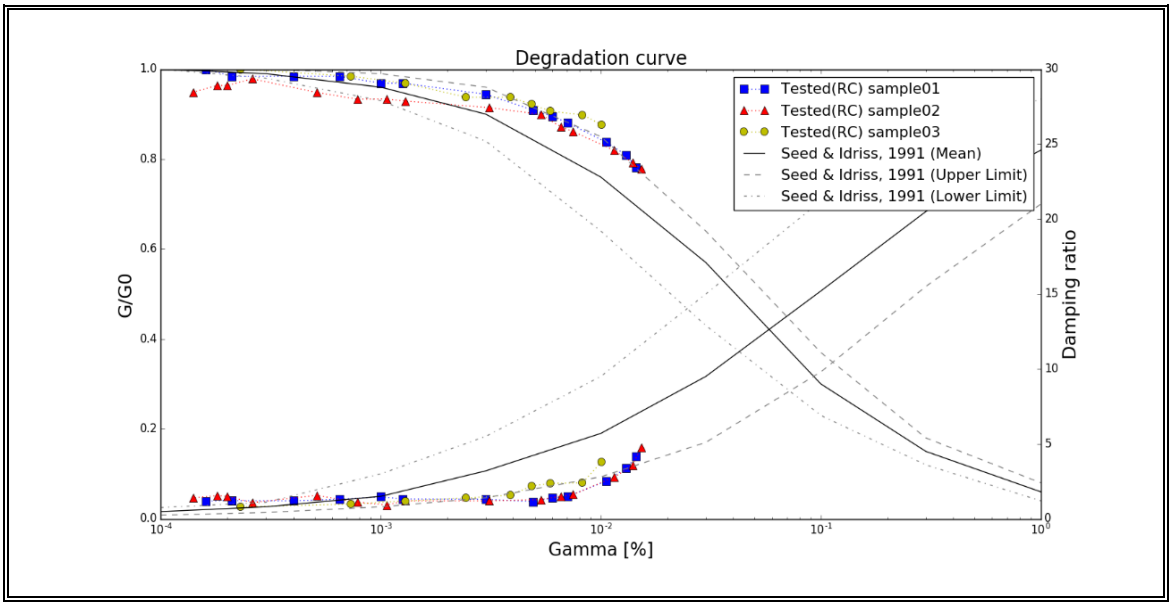

Figure 2.6: normalized modulus reduction and damping curves from RC tests for the uniform particle-size

Figure 2.6 shows the degradation of this material, particularly it can be inferred this material is rigid in comparison with Seed & Idriss 1991 reference curves.

2.6.2 Torsional shear tests

Figure 2.7 illustrates the results of a test in which a cylindrical uniform specimen of a glass beads with 40% relative density was isotopically consolidated under 100 kPa stress, followed by cyclic undrained shear loading. It is found therein that the degradation curve of the uniform gradation samples tested at different loading frequencies shows the same behavior.

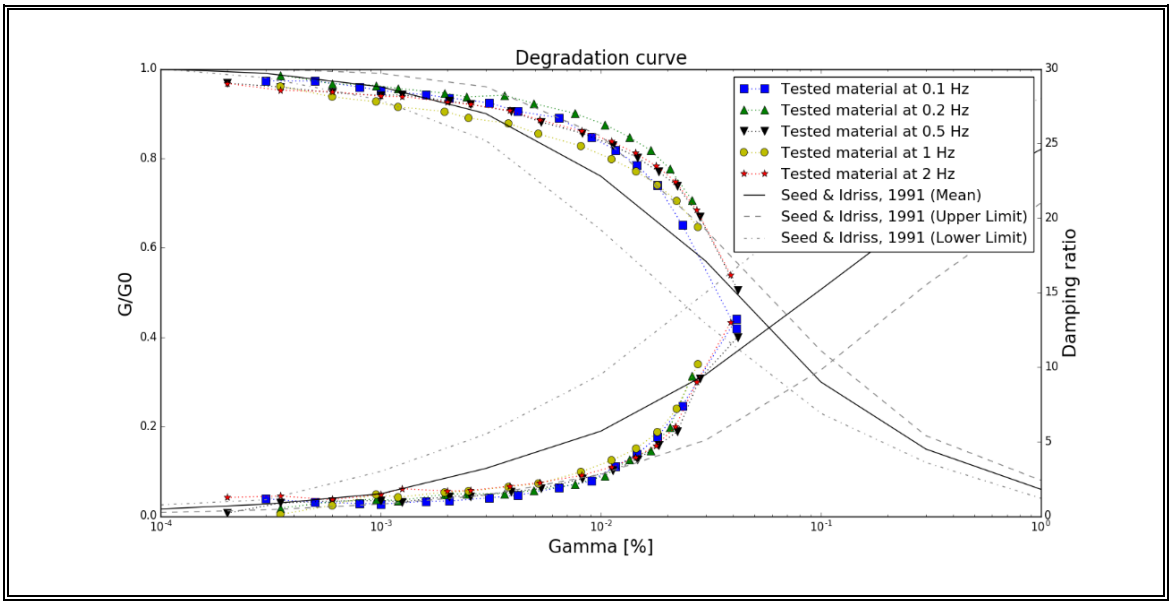

Figure 2.7 normalized modulus reduction and damping curves from TS tests for the uniform particle-size

It can be noted that the Torsional Shear test reaches a higher level of strains that the Resonant Column test. In relation with the comparison between this results and the Resonant Column test, it can be seen a similar behavior in terms of degradation of shear modulus and damping in the same range of strains (Figure 2.8).

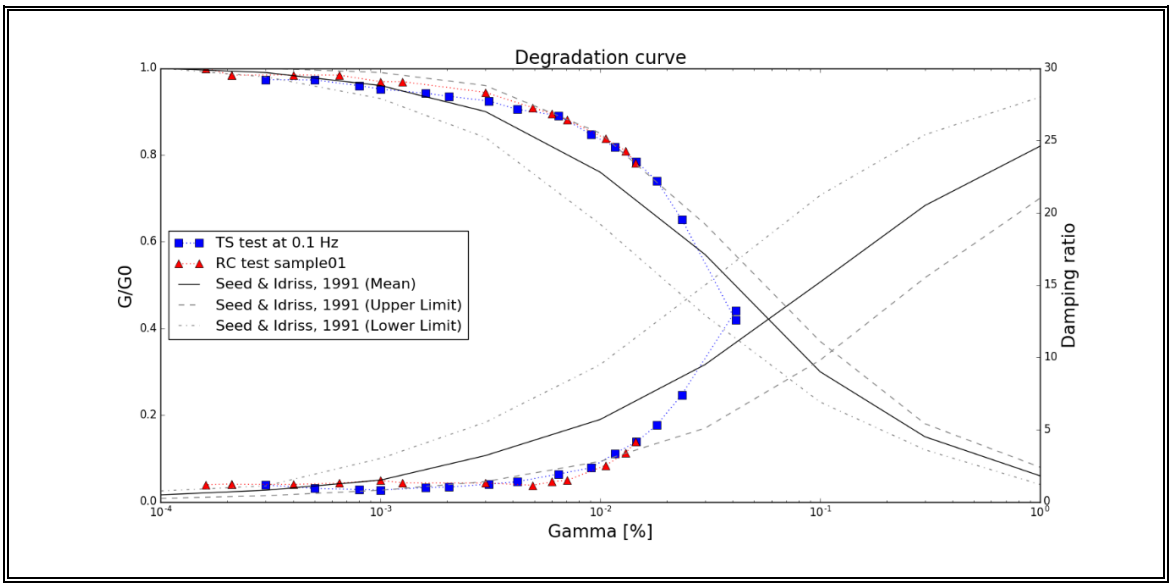

Figure 2.8: comparison between normalized shear modulus reduction and damping curves from RC & TS tests for the uniform particle-size at 100 kPa of confinement

There were also conducted Torsional Shear tests with the same sample properties at a higher confinement of 200kPa (Figure 2.9), showing approximately the same response for different frequencies.

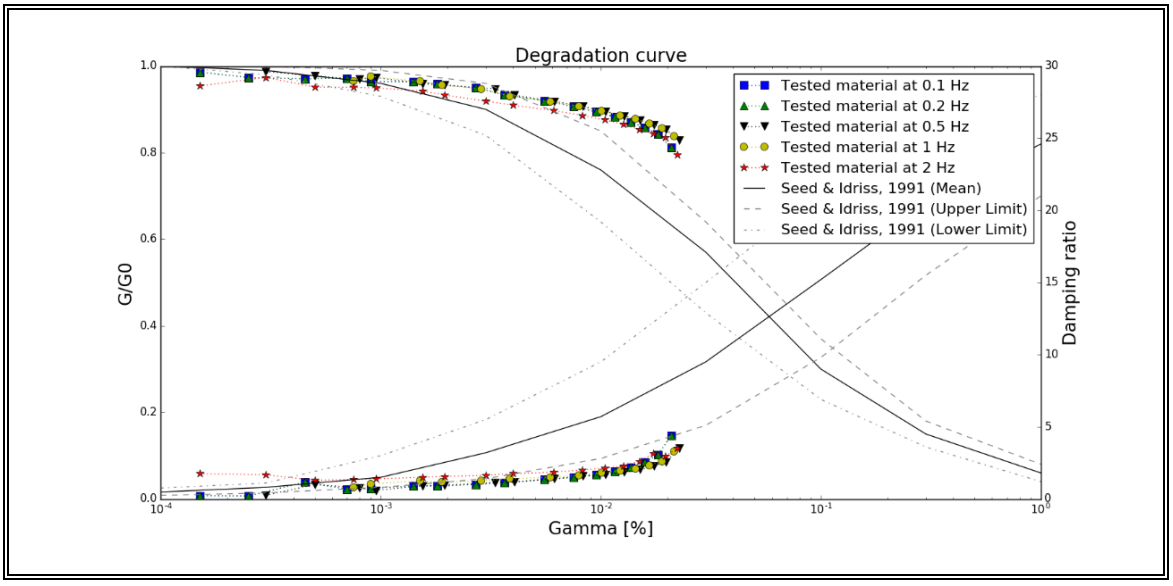

Figure 2.9: normalized modulus reduction and damping curves from TS tests for the uniform particle-size at 200kPa confinement

In the Figure 2.10 it is compared the results of torsional shear test for the uniform sample at different confinement pressures. It can be observed an increment of the stiffness and a reduction increase of damping accordingly to the increase of effective stress.

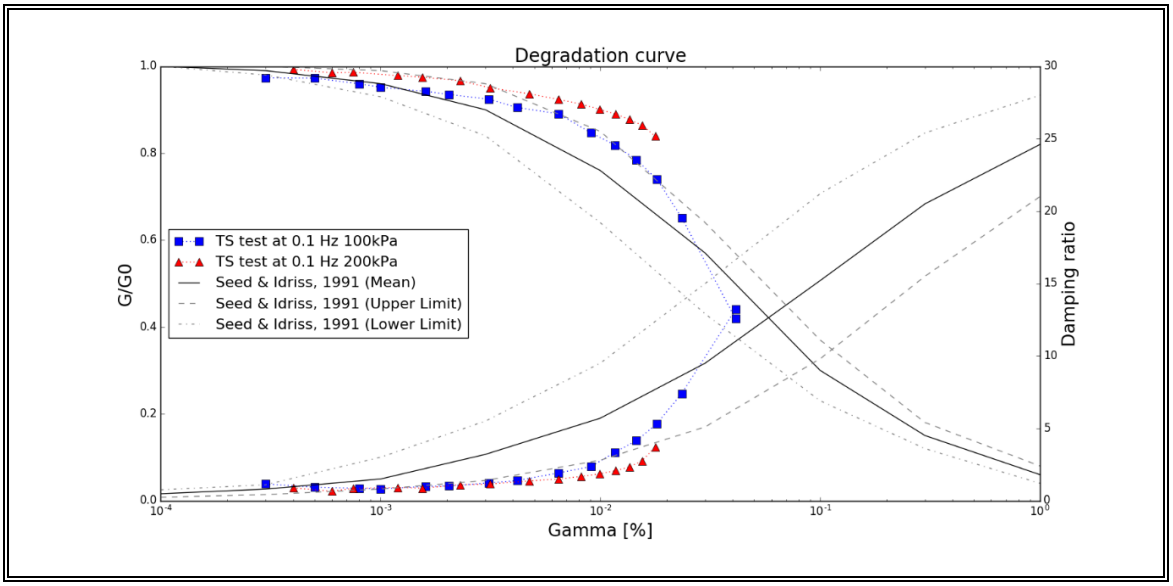

Figure 2.10: comparison between normalized modulus reduction and damping curves from TS tests at 100 and 200 kPa for the uniform particle-size distribution

Finally, it is tested the non-uniform grading distribution in order to study the effect of grain size in material degradation and damping amplification. Figure 2.11 shows the comparison between torsional shear tests applied to both particle size distribution samples at 0.1 Hz.

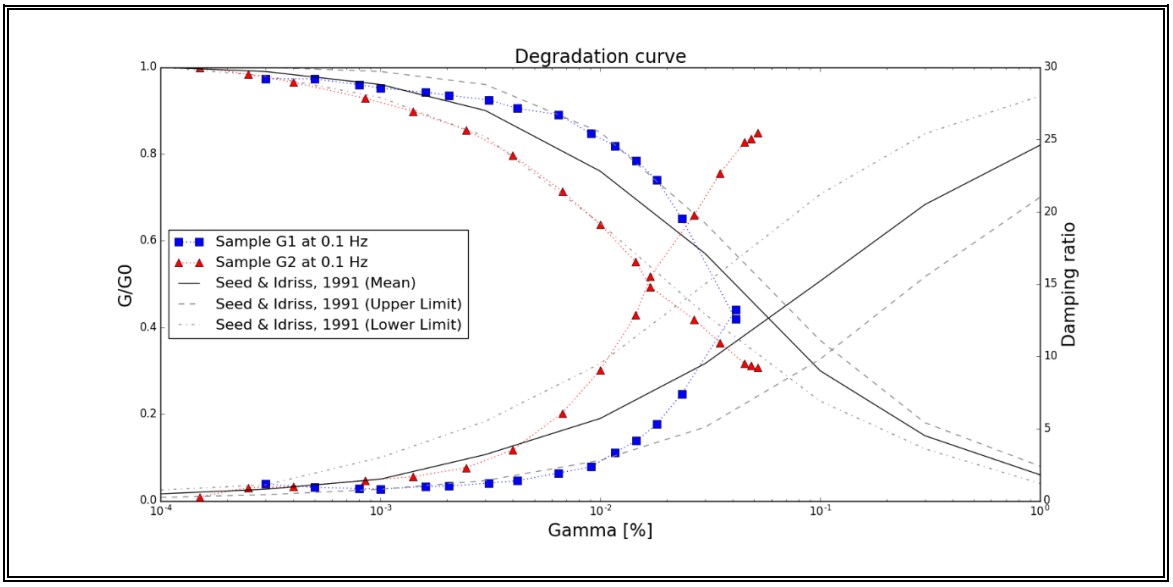

Figure 2.11: comparison between normalized modulus reduction and damping curves from TS tests at 100 KPa for the uniform and non-uniform particle-size distribution

It can be seen the shear modulus degradation and damping increase in the non-uniform sample occurs earlier than the uniform sample. In other words, the non-uniform sample starts having plastic deformations (particles movement due sliding and structure arrangement) at lower strains than the uniform sample. This behavior is reflected by a sharp increase of damping ratio. The increase of the inelastic component of the response can be illustrated through the comparison of the hysteresis loops for both samples at the same confinement and strain amplitude as it is shown in Figure 2.12.

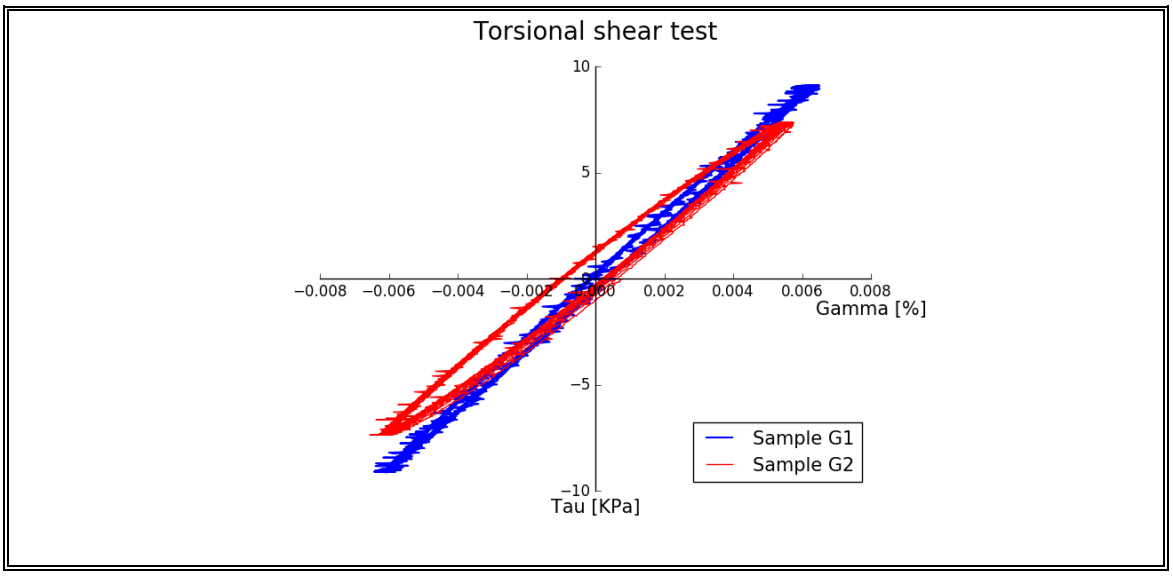

Figure 2.12: comparison of hysteresis curves from samples for the uniform and non-uniform particle-size distribution

The results discussed in this chapter will form the basis for calibration of the micro-mechanical model presented in Chapter 4 that will allow to study the uniformity of strain distribution during cyclic shear test.

3. DISCRETE ELEMENT METHOD

3.1 Overview

The philosophy behind the DEM is to model the actions that happen at a microscopic level and study how these actions affect the evolution of the motion of a whole granular media in a macroscopic level. This method needs mainly a contact detection strategy, time-discretized equations of motion governing the particle displacements and interaction laws describing the inter-particle relations.

A DEM analysis starts with a collection of particles or by creating particles in a designated region. Either a sphere or another geometrically well-defined volume or a combination of them mathematically represents each physical particle. The movement of these spherical particles is based on the corresponding momentum balances. Along with the current position and velocity of a particle, the particles physical characteristics are used to calculate the current forces upon the particle. The forces typically include gravity, friction, and pressure from contact with other particles and physical system boundaries that may include other effects such as those caused by cohesion. These forces are then used to predict the particles future location and velocity for some minor increment called the time-step. Normally the time-step is on the order of millionths of a second. This process is repeated for every particle in the system for each time step.

The basic law that rules DEM problems is the Newton's Second Law, which governs the motion of bodies interacting with each other under the action of various forces. The other crucial physical fact modeled by this method is the impact between 2 bodies, an action that is going to take place several times in the computations providing the most important information for the problem being solved.

When the two bodies start the contact, the energy can be dissipated in terms of sound, deformation, vibration and heat. Depending on the material, the deformations could reach the plastic state and be permanent. The force created in these contacts is essential to compute the stresses and strains affecting the particles of our system. In order two study the interaction of particles through the contacts, different models have been created proposing strategies to solve these situations each one offering different output.

3.2 Normal contact law

This law will provide the information related to reaction normal forces (F_n) due contact and impacts between particles in DEM simulation. This relation is involved in all the processes that control the granular assembly and conjugate the particles interpenetration with the repulsion force. The two most used contact models are:

- Linear contact model: The standard contact law model for granular materials is shown in Eq. (3.1), where the magnitude of the forces is the product between the interpenetration (δ_n) and the user defined contact stiffness (K_n). The direction of this force is oriented such that the reaction forces are aligned to the line joining the center of the two contacting particles.

$$F_n = K_n \delta_n \qquad (3.1)$$

  Although spring constants used in this model can be calibrated in order to replicate overall response of the assembly, the spring constants cannot be directly related to the material properties of the solid particles. Then, the deformation of particles is not related with the material stiffness. In this way, this model is more suitable for 2D and quasi-static problems (Latzel, Luding, & Herrmann, 2000).

- Hertzian contact model: This law suppose two rigid and elastic spheres with specific young modulus, radius and velocity. It states the relation between the compression or overlap of the particles and the force created when they are in contact. Particularly, the normal pushback force between two particles is proportional to the area of overlap between the two particles. The contact force generated by the contact of these two particles will be a straight line passing through the point where they established contact and the gravity centers of the particles. This model relates the magnitude of the force to the contact area and the material properties, consequently the force is not linearly related with the interpenetration (Hertz, 1882).

The normal contact force is calculated from the individual properties of the particles in contact. To take into account this individual properties, equivalent Young´s Modulus ($\bar{\bar{E}}$) and radius ($\bar{\bar{R}}$) are used (Eq. 3.2).

$$F_n = (\frac{4}{3}\bar{E}\sqrt{\bar{R}})\delta_n^{\frac{3}{2}} \qquad (3.2)$$

$$\frac{1}{\bar{\bar{E}}} = \frac{(1-v_i^2)}{E_i} + \frac{(1-v_j^2)}{E_j} \qquad (3.3)$$

$$\frac{1}{\bar{\bar{R}}} = \frac{1}{R_i} + \frac{1}{R_j} \qquad (3.4)$$

The main difference between these two models is that linear laws consider the overlap as single dimension parameter, while the Hertz model uses the contact area, which is a two dimensional quantity. This difference leads to that Hertz's force quickly exceeds a linear relationship, although a high linear stiffness is used. When high confinements are used, the linear contact allows larger overlaps than the Hertz's model, which might change the problem's mechanics.

3.3 Tangential contact law

The shear forces or tangential forces refer to the component of the force that acts along the contact surface. Theoretically, two smooth spherically perfect particles cannot develop frictional resistance since the contact surface is a single point. However, DEM models include a frictional parameter in order to represent the resistance generated by the interaction and interlocking of asperities on the rough surface of the particles.

Before particles start sliding, there is an increment of forces until the point of yielding or gross sliding. The simplest approach to define the initiation of gross sliding is to assume Coulomb friction model, where shear force is calculated from normal contact force limited by the friction coefficient μ. Then, sliding occurs when the friction is completely mobilized and the tangential force (F_t) reaches it maximum value (Eq. 3.5).

$$F_t^{max} = \mu |F_n| \qquad (3,5)$$

The Hertz-Mindlin contact model, is a set of non-linear contact formulations which includes the approximate model used to calculate tangential forces as it is shown in Eq. 13 (Mindlin and Deresiewiez, 1953). The advantage of this formulation, as the Hertzian contact model, is that includes the material properties of the particles in the calculation of the reaction force. Equivalent shear modulus $\bar{\bar{G}}$ calculation is shown in Eq. 3.6 and 3.7.

$$F_t = 8\bar{G}\sqrt{\bar{R}\delta_n}\delta_t \qquad (3.6)$$

$$\frac{1}{\bar{G}} = \frac{2(2+v_i)(1-v_i)}{E_i} + \frac{2(2+v_j)(1-v_j)}{E_j} \qquad (3.7)$$

3.4 Time step

The idea of time integration is that knowing the position and acceleration of a body we can predict its future displacement. The time step has to be small enough to assure the system stabilization and model convergence. The smaller the time evolution, the associated analysis and calculation will be more refined and will approach to continuous analysis but the computational cost increase. For this reason, there are different methods to find an optimal time step.

In this study, it was used the Hertz approach since it was used a Hertz-Mindlin contact model. This criteria considers the particle's maximum speed (v_{max}) and the equivalent mass ($\bar{m}$) as indicated in Eq. 3.8. To determine the critical time step (maximum stable time step), the collision of each particle is considered, and the smaller time step is used:

$$t_{crit} = 2.87\sqrt[0.2]{\frac{\bar{m}}{\bar{R}\bar{E}^2 v_{max}}} \qquad (3.8)$$

$$\frac{1}{\bar{m}} = \frac{1}{m_i} + \frac{1}{m_j} \qquad (3.9)$$

3.5 Stress and strain calculation

To compare micromechanical results with standard macroscopic strain and stress values, some rules to compute those quantities must be selected. This homogenization is not straightforward, because involves the relation between a discrete media to an equivalent continuum material and some important mechanics that operate at particle scale cannot be properly captured by a continuous approach.

3.5.1 Particle stress calculation

Equation 3.9 shows the particle stress (σ_{ij}^{p}) calculated from contact forces (f_j^c) in direction from the particle p to centroid to contact point c over the particle volume (V_p).

$$\sigma_{ij}^{p} = \frac{1}{V_p}\sum_{c=1}^{N^{c,p}} |x_i^c - x_i^p| n_i^{c,p} f_j^c \qquad (3.9)$$

Where $|x_i^c - x_i^p|$ is the distance from the contact point (x_i^c) to the center of the particle (x_i^p), represents the radius in spherical particles.

3.5.2 Local stress calculation

For the calculation of local stress ($\bar{\sigma}_{ij}$) (Eq. 3.10) it was used the method proposed by Potyondy and Cundall (2004) which considers an adjustment of the measurement volume (V) by the sample porosity (n) as it is presented in Eq. 3.11.

$$\bar{\sigma}_{ij} = \frac{1}{V}\sum_{p=1}^{N_p} \sigma_{ij}^{p} V_p \qquad (3.10)$$

With,

$$V = \frac{\sum_{p=1}^{N_p} V_p}{1-n} \qquad (3.11)$$

To define the measured volume it was taken a vertical slice of 6 mm thick, then the slice was vertically divided into 10 rectangular strips of 1cm tall and 5 cm width. All particles with centroids within the volume where considered as a whole in this calculation.

3.5.3 Local shear strain calculation

The local shear strain is calculated, as the local stress, using a measurement volume in which are considered all the particles with their center therein. Then, it is calculated the average displacement of the group of particles around the vertical axis. To achieve this, first it was necessary to change the reference system to cylindrical coordinates in order to have a direct calculation of the angular displacement of each of the particles. Thus, it is obtained a macroscopic value for shear strain calculated from microscopic parameters.

For building the stress-strain curves it is considered a secant shear strain value associated to the maximum twist angle at the top of the sample (clump twist), which is easy to obtain using the method mentioned previously. That is to say, for hysteresis loops calculations it is used an average shear strain under the hypothesis of linear strain distribution. Finally, to calculate the strain it is considered 0.8 times the sample radius and its height as it is explained in the point 2.2.

Finally, using the average twist angle of the particles at different heights, it studied the shear strain distribution in the sample using its theoretical definition presented in Eq. 3.12.

$$\gamma = r\frac{\partial\theta}{\partial z} \approx r\frac{\Delta\theta}{\Delta z} \qquad (3.12)$$

The considered radius (r), as the previous calculations, is 0.8 times the sample radius. In the case of $\Delta\theta$ it is considered the difference between average twist angle of the particles at the top of each control volume with it corresponding value at the bottom of such. While Δz it is a constant value equal to 1 cm, which corresponds to the width of the control volume previously mentioned.

3.5.4 Shearing velocity

Since the cyclic loading was applied due angular deformation, the shearing velocity was controlled through the twist angle $\theta(t)$ which was described as a sinusoidal function (Eq. 3.13) in order to avoid any inertia effect on the resulting hysteresis loop when rotation sense changes. The applied twist velocity was controlled to minimize the effects of kinetic energy on the simulated G and D values. The angular distortion is defined by the amplitude θ_0 and the rate of rotation (frequency f equal to 0.1 Hz), hence the computational time (t_0) necessary to reach the maximum required rotation can be calculated from Eq. 3.14.

$$\theta(t) = 2\pi t \frac{\theta_0 \sin\left(\frac{0.5\pi t}{t_0}\right)}{2\pi t} \qquad (3.13)$$

$$t_0 = \frac{\theta_0}{2\pi f} \qquad (3.14)$$

3.6 Software and visualization

3.6.1 LIGGGHTS Code

Why LIGGGHTS? This software was chosen for this study because it is free, easy to use, its source code is well structured, easy to understand and modify. It is also fast and

it is suitable for massively parallel computing. Another big advantage is that is well documented and it has large user community.

LIGGGHTS is an open source, MPI parallel DEM code written on C++ for modelling granular materials. LIGGGHTS stands for **L**AMMPS **I**mproved for **G**eneral **G**ranular and **G**ranular **H**eat **T**ransfer **S**imulations (CFDEM.com, 2016). This code was developed by Christoph Kloss of Christian Doppler Laboratory on Particulate Flow Modelling at Johannes Kepler University, Austria.

This code is based on LAMMPS and it provides potentials for modelling soft materials, solid-state materials and coarse-grained granular materials. It can be used to model particles at the atomic, granular or continuum scale. Given the boundary conditions LIGGGHTS simulates the materials by integrating Newton's equations of motion for a system of interacting particle's forces.

LIGGGHTS offers both linear and non-linear granular potentials for modelling DEM methods which involve the simulation of coarse-grained granular particles. All these features of LIGGGHTS for granular simulations are improved from LAMMPS.

The following are some of the features that LIGGGHTS improves on LAMMPS:

- It is possible to import complex geometry from computer-aided design (CAD) into a LIGGGHTS simulation
- Pair style parameters like stiffness and damping can be linked to material properties that can be derived from lab experiments (e.g. density, Young's Modulus, Poison's ratio and coefficient of restitution)
- It has the potential to model macroscopic cohesion
- LIGGGHTS has Dynamic load balancing

3.6.2 Paraview

LIGGGTHS does not do any post processing or visualization of the simulations. However many visualization tools available can be coupled with LAMMPS to visualize the output.

The one used this study is Paraview (paraview.org, 2016). ParaView is an open-source, multi-platform data analysis and visualization application. The data exploration can be done interactively in 3D or programmatically using ParaView's batch processing capabilities. ParaView was developed to analyze extremely large datasets using distributed memory computing resources (paraview.org, 2016).

The post processing stage consists of two separate steps. First, is to extract the snapshot of the simulation from the dump files created by LAMMPS. The dump file contains the energy of each particle for every specified frame. It is a tough to read the information from the dump file manually.

Then, it is necessary to extract the contact forces and position information from every contact. With this, it can be calculated and analyzed all the information needed using another tools. For this study, all the codes used were own-programmed using MATLAB and Python.

3.7 Material modeling calibration

In order to calibrate the micro-parameters controlling the global behavior of DEM simulations, the first part of the investigation is devoted to reproduce the experimental response of the considered material on direct shear test. Thus, similarly to the work of Salazar et al. (2015), it is used a 3D DEM model to calibrate the particle contact friction. Once the friction parameters were calibrated, it was developed the cyclic torsional shear model in order to study the stress and strain distribution during this test at a micro-mechanical level.

A summary of the calibration described above and the work conducted to reproduce the cyclic torsional shear test by 3D DEM modeling is presented in the following chapter which has been submitted to Acta Geotechnica Journal.

4. CYCLIC TORSIONAL SHEAR TEST MODELLING

STUDY OF THE STRESS AND STRAIN DISTRIBUTION IN THE CYCLIC TORSIONAL SHEAR TEST BY DISCRETE ELEMENT MODELING

4.1 Abstract

In this research, a torsional cyclic shear test was modeled using the 3D discrete element method (DEM). The results are compared against experimental data and micro-mechanical aspects of the soil during the loading are discussed. The aim of the work is to study the homogeneity of strains during this laboratory test, and to compare the micro-mechanical behavior of the soil sample for different strain levels.

The experimental investigation was performed using a synthetic soil material made of glass beads, which simplifies the modelling and calibration since normal interaction forces do not induce rotation of the particles. Both the model and experimental tests used the same grading distribution and particle size.

We showed that the hysteresis cycles can be properly reproduced in terms of shape and magnitude. Thus, we obtained a robust estimation for the secant shear modulus and damping ratio at different strain levels. With this, it was possible to build a stiffness degradation and damping increase curve and to compare it with experimental data obtained from torsional shear tests. Based on this validation of the DEM model, we discuss the micro-mechanical behavior of the soil and its relation with the macroscopic parameters obtained. It is shown that shear strain distribution on the sample becomes relatively larger close to the top of the sample as top rotation increases, which differs from the standard assumption of uniform strain distribution. Additionally, it is observed that at 0.8 times radius, the cumulative torque reaches approximately 90% of the total torque applied to sample.

Keywords: DEM, Cyclic Torsional shear test, micro-parameters, glass beads, Shear modulus.

4.2 Introduction

In this paper, a 3D Discrete Element Method (DEM) model of the cyclic Torsional Shear (TS) test was developed to reproduce the response of glass beads with the main purpose to explore the distribution of stresses and strains in the sample at different levels of deformation. The goal is to directly use the physical and mechanical properties of particles provided by the manufacturer for the DEM simulations. The ability of this modelling approach to reproduce experimental data is discussed in terms of hysteresis loops, shear modulus degradation and damping ratio evolution.

The TS test is widely used in earthquake geotechnical engineering to investigate the response of soils to cyclic loads. The soil properties that can be estimated with this test are basically the secant shear modulus and damping ratio in terms of the applied distortion. For example, both of them are used in earthquake geotechnical studies to anticipate site amplification effects.

The test outline consists in a cylindrical sample of soil and a rigid mass on the top of it, which is summited to a cyclic torsional force while the bottom is fixed (Fig 1). Imposing a cyclic torsional excitation at the top of the sample, it is possible to measure stiffness and damping characteristics over a small strain level range (10^{-6}-10^{-3}) [23].The dynamic response of a specimen to this force is measured in terms of the angular acceleration and/or displacement at the top of the sample.

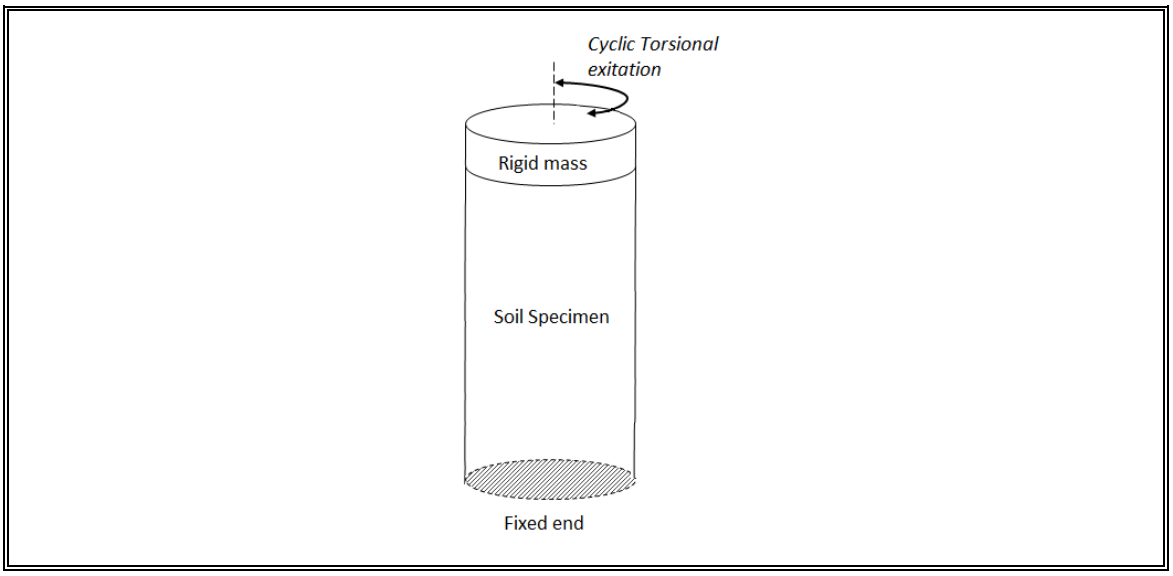

Figure 4.1: Schematic representation of the Torsional cyclic Shear test (TS)

Several studies have been carried out using DEM to investigate soil behavior during elementary laboratory tests (e.g., Cui and O´Sullivan [5]). For monotonic loading tests, O'Sullivan [16] gives an excellent guide for DEM modelling for researchers to understand fundamental soil mechanics. In the case of cyclic loading tests, a limited number of studies have been made. Most of them simulated biaxial compression assemblies [20] aiming to investigate the response of shear modulus and damping ratio under cyclic loading. O'Sullivan [14] replicated cyclic triaxial tests using a three dimensional stress controlled membrane, achieving good results and properly capturing the trend of variation of stiffness with strain.

Later, L. Tong & Y. H. Wang [22] developed a model of a 3D cyclic shear test using a nonlinear contact model and clumped particles. They were able to reproduce the hysteresis loop with the model and to compare their results against experimental data, analyzing the damping ratio and shear modulus at different strain levels delivered from either traced energy or resulting hysteresis loops.

For conventional triaxial compression tests, it becomes necessary to replicate the confinement effect modeling a membrane. One common strategy is the stack wall replacement presented by Zhao X. and Evans T.M. [25], which consists in simulating

multiple membranes using stacks of planar strain conditions or cylindrical compressive walls that could deform independently of one another. Using this strategy, Bo Li [10] reproduced the triaxial confinement effect using the technique applied to a cylindrical sample. This model consisted in a torsional shear test with a hollow cylinder shape, where the torque applied to the specimen is simulated through an angular velocity applied to the soil particles near the top boundary.

Other efforts were focused on using strings of bonded particles in order to simulate flexible membranes, however they showed difficulties in implementing a cylindrical membrane which deforms both axially and radially. In the case of this study, the axial component of deformation is not relevant.

A good example of this type of strategy is the work of De Bono [4], who used this technique to reproduce a flexible membrane for triaxial testing. This study used a cylindrical array of particles that encased the soil sample; this group is bonded in such a manner that it transmits no moments, ensuring membrane flexibility [4]. Each particle is generated 1/3 smaller than the smallest sample particle and then subjected to a discrete force in order to replicate the confinement pressure. The results of this work shows that the behavior of the soil specimen under pure torsional stress state can be reproduced with discrete element simulations, since an evolution on stress and the coordination number after applying a torque can be seen.

Although this investigation achieves a good representation of a confinement effect, we were limited to using the linear springs contact model. A Hertz-Mindlin contact model is used in this study in order to better capture the confinement effect on the sample stiffness and consequently the resulting shear modulus degradation and damping increase.

4.3 Laboratory tests

4.3.1 Tested material

The selected material was a synthetic soil made of glass beads. It was selected because of its simplicity for further analyses and calibration with the DEM model. The

main feature of this aggregate is that it can be modelled as a spherical particle without any particular consideration, to take into account grain rotation due to eccentricities of normal forces; this reduces the parameters which must be calibrated and simplifies the numerical calculations. The properties of this material are shown in Table 4.1. Three density tests were done in order to check the specific gravity of the solid, obtaining a value of Gs equal to 2.5. The rest of the mechanical properties where obtained from the product's technical datasheet.

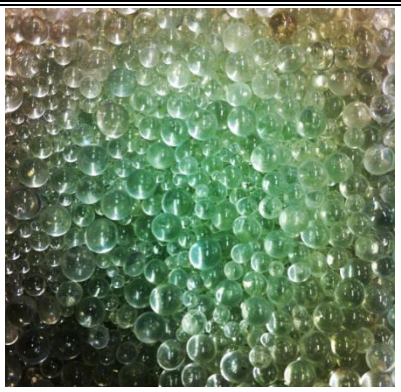

Figure 4.2: Synthetic material made of glass beads

Table 4.1 properties of tested material

Property	Value
Particle Density: γ (kN/m^3)	25.0
Young's Modulus: E (GPa)	63
Poisson coefficient: υ	0.265
Cohesion: c'(kPa)	0

Regarding the particle size distribution, first, beads with diameters between 2.85 and 4.4 millimeters were used in order to have an approximate uniform distribution with all the material retained in sieve #8 (G1). Since this material is provided in packages with

different ranges of size, three packages were used which contained particles bigger than 2.38 mm but smaller than 4.4 mm. A second non-uniform grading distribution was studied to assess the role of grain packing in both experimental results and DEM modeling (G2). The proportions used for the different packages are shown in the Table 4.2. The associated grading curves are displayed in the Figure 4.3a. Both grading curves were chosen accordingly to fractal distributions since this kind of grain size distribution is the most frequent in natural materials.

Table 4.2 particle size distribution of the tested material

Diameter range (mm)	Percent of total weight (%)	
	G1	G2
3.8 - 4.4	27.6	12.4
3.4 - 4.0	38.0	17.1
2.85 - 3.45	34.4	15.5
2.4 – 2.9	-	15.4
2 – 2.3	-	7.8
1.7 – 2.1	-	6.2
1.55 – 1.85	-	7.8
1.25 – 1.65	-	9.3
1 – 1.3	-	8.5

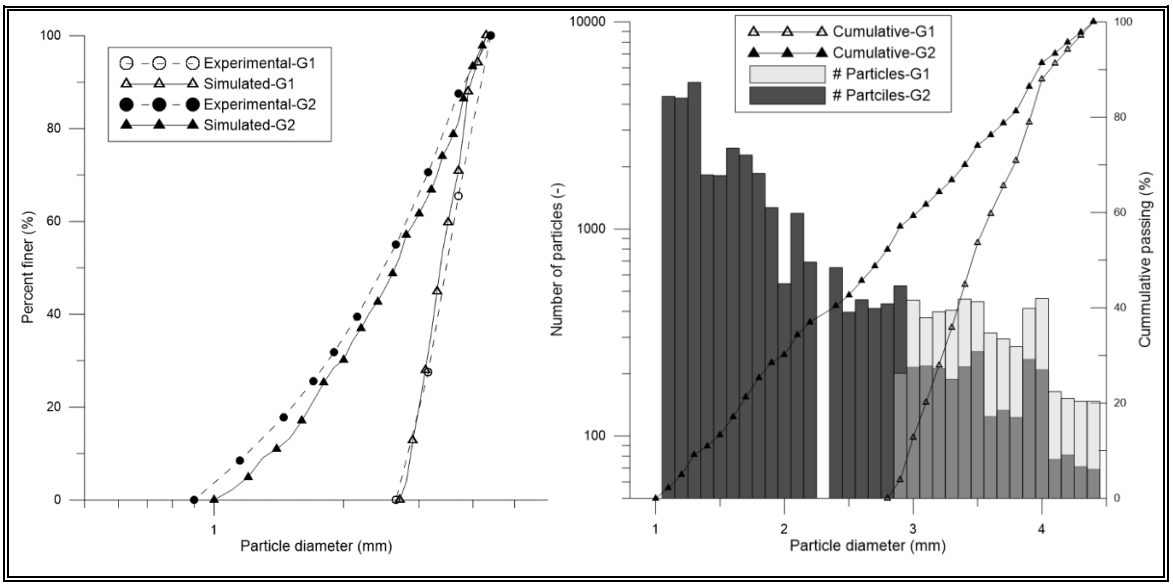

(a) (b)

Figure 4.3: distribution of grain sizes: (a) experimental and simulated grading curves (b) simulated particle size histogram

The uniform material (G1) was classified according to the Unified Soil Classification System (USCS), resulting in a poorly graded sand (SP) because all the particles are retained in sieve #8. Meanwhile, the non-uniform sample (G2) was tested with grains distributed in sieves #8, #16 and #30 where a 0.65, 0.31 and 0.085 percent of the total weight respectively was retained, resulting also in a poorly graded sand with Cu equal to 4 and Cc equal to 1.

Moreover, physical properties for both samples were obtained from density tests (minimum and maximum). For the uniform distribution, the maximum and minimum void ratios were obtained from a maximum density test. A maximum density of 15.5 (kN/m^3) and a minimum density of 14.8 (kN/m^3) were measured for G1 and 16.7 (kN/m^3) and 15.7 (kN/m^3) respectively for G2. A 40% of relative density was selected for the study, with an associated void ratio of 0.66 for G1 and 0.55 for G2, which corresponds to relatively loose sand in both cases. Finally, the angle of internal friction was estimated from both triaxial and direct shear tests by adjusting the Mohr-Coulomb failure criterion to the results. The properties of the synthetic soil samples are summarized in the Table 4.3.

Table 4.3 properties of synthetic material

Property	G1	G2
Density: γ (kN/m^3)	15.1	16.1
Void ratio: e_0	0.66	0.55
Angle of internal friction: $\varphi°$	26	32
Cohesion: c'(kPa)	0	0

4.3.2 Specimen preparation

The material was dried in an oven and separated in capsules with the exact amount of material to fill the Torsional Shear (TS) device mold (50 mm diameter and 100 mm height), according to the selected relative density. The sample was introduced in a cylindrical mold with the latex membrane wrapped inside. Both of these elements were attached to the fixed porous metal in the base of the Resonant Column (RC) device.

The filling procedure was made according to the ASTM D4015 procedures. The material was deposited in 5 layers inside the mold using a funnel. Since the relative density of the sample is low, it was not necessary to compact every layer to obtain the density required. After the material was placed into the mold, it was sealed in the top using rubber rings along the rigid mass on the top of the sample; vacuum is applied to keep the shape of the specimen while the equipment is assembled and a cell pressure is applied. The sample was then filled with de-aired water flowing from the bottom through the porous stone. It is important to highlight that the use of glass beads is very convenient in terms of laboratory time since this material saturates and consolidates very fast because of its high porosity and lack of fines. The saturation process was done in steps of 20 (kPa) loading increments until it reached a 95% of saturation according to B parameter of Skempton. Then the sample was consolidated with effective pressure of 100 (kPa) and then tested with the same confinement pressure

4.3.3 Cyclic Torsional shear test results

The tests were performed using the combined RC/TS apparatus from CONTROLS™ available in the Geotechnical Engineering laboratory at Pontificia Universidad Católica de Chile. This unit combines the features of both resonant column and torsional shear tests into a single device.

The resonant column apparatus includes a current-driven motor to apply torsional load to the sample, a series of transducers for signal conditioning, a cell, a back pressure electro pneumatic control system and a data logger.

Since this device has a transductor for angular rotation, the average shear strain amplitude is usually calculated under the hypothesis of linear distribution of deformations (ASTM D4015-92). Particularly, the angular distortion is calculated as the product of radius and twist angle divided by the specimen height. The torsional shear test is typically conducted in undrained conditions, to measure and evaluate the changes in pore water pressures.

Cyclic torsional shear tests were performed using the equipment mentioned above with confinement pressure of 100 kPa. The tests were conducted at different amplitudes and frequencies, keeping the number of loading cycles constant and equal to 20. Each sample was submitted to a set of frequencies of 0.1, 0.2, 0.5, 1 and 2 Hz. For higher frequencies, the normalized shear modulus remained constant, while the damping increases as well as the frequency. The purpose of conducting this test at different frequencies was to evaluate the capabilities of this device and the response of this material at different loading rates, as well as to investigate the ability of the DEM model to reproduce those variations.

Shear modulus and Damping are calculated from hysteresis loop. The starting data used by the TS software are the sample stimulus and the response in torque (T_r) which is acquired in Volt and converted internally to Ampere by a calibration constant. The stimulus is a pure sinusoidal signal, preceded by a half period of zeroes to calculate the offsets. The calculation starts subtracting these offsets from the arrays, thus centering the sinusoidal signals on the horizontal axis. The next step is converting the electric stimulus

into shearing stress (Eq. 4.1) by multiplying the coil current output by a calibration constant (k), and dividing by the specimen polar moment of inertia (J_p) and its radius (R). Finally the response in strain (Eq. 4.2) is commonly approximated by the measured angular twist (θ), specimen radius (r) and specimen height (l). In this case we suggest using 0.8 times the radius ($r = 0.8R$) in order to have a presentative shear strain for a given specimen.

$$\tau = R\frac{kT_r}{J_p} \qquad (4.1)$$

$$\gamma = r\frac{\partial\theta}{\partial z} \approx \theta\frac{r}{l} \qquad (4.2)$$

The range of strain amplitudes explored for each frequency was between 10^{-4} % to 4×10^{-2} %. Experimental results of TS of the synthetic material are compared against reference results for sands from Seed & Idriss (1991) in Figure 4.4. In the case of the uniform grain size distribution, Figure 4.4 indicates that modulus reduction and damping curves are almost independent of the rate of loading in the explored range of frequencies, nevertheless damping values are more stable than shear modulus defining a very narrow curve. In the case of the non-uniform grading curve, stiffness degradation values are very stable, but damping tends to be larger at 0.1 Hz compared to 0.2 Hz. Nevertheless, differences are very low for practical purposes. In relation to reference values for sands, the shear reduction curve obtained for the uniform case shows stiffer behavior for strains larger than 0.002%, when experimental values are closer to the upper limit as suggested in Seed & Idriss (1991). On the contrary, for this particle size distribution, damping values follow the reference lower limit up to 0.02%. For strains larger than this value, the damping ratio grows drastically and comes close to the reference upper limit. In the case of the non-uniform particle size distribution, the stiffness degradation curve approximately follows the reference lower limit, but damping grows drastically at 0.004% and exceeds the reference upper limit for strains larger than 0.02%. Because non-uniform material shows more stiffness degradation compared to uniform case, larger strains could be explored for maximum torque that could be imposed by the experimental device. Nevertheless, maximum shear moduli are about 155 GPa and 135 GPa for the non-uniform

and uniform cases, respectively. In general terms, experimental data agrees satisfactorily with usual curves for clean sands.

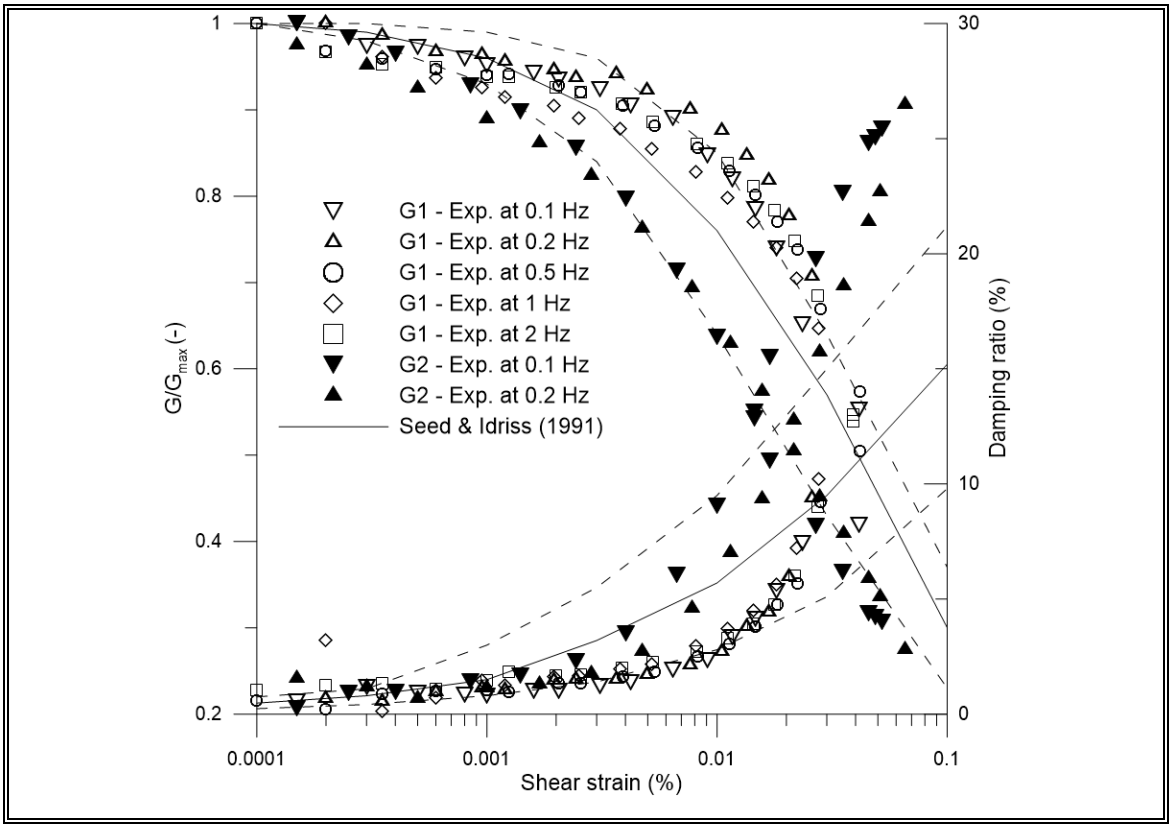

Figure 4.4: experimental stiffness degradation and damping curves for both particle size distributions.

4.4 DEM simulations

4.4.1 Discrete material

DEM simulations were run with the free software LIGGGTHS which is a 3D open source code implemented with several granular features such as the Hertz contact model which was used in this case. This algorithm was run with a dynamic time-stepping procedure to analyze the soil as an assembly of individual particles, calculating the movement and forces interactions between them and external objects or boundaries. This

methodology allows having control of the position and interaction forces of the whole medium, permitting a micro-mechanical analysis of the material.

The DEM material consists of a three dimensional assembly of spheres with elastic properties, as listed in Table 4.4. These properties were chosen according to the work of Salazar et al. [19] and from the product's technical datasheet, with the exception of friction parameters. No rolling friction is considered because synthetic soil particles have a spherical shape.

The laboratory test conditions and DEM input parameters were consistent for both direct shear and torsional shear tests. The particle size distribution is modeled with the same diameter intervals as the tested material (Table 4.2). The difference between the tested particle distribution and model particle distribution is given by the random diameter generation in each interval (Figure 4.3b).

Regarding the contact friction between particles, it becomes necessary to differentiate three different type of particles - Soil, Clump and Membrane - which will interact between each other with different friction coefficients. The contact friction between soil particles was calibrated based on a Direct Shear DEM model for the uniform case (G1), comparing these results with experimental data similarly as described in [19]; the rest of friction parameters were calibrated using the Torsional Shear DEM model developed in this work.

Table 4.4 properties of modeled material

Property	Value
Young Modulus: E (GPa)	63
Poisson ratio: υ	0.256
Particle density: ρ_p (kg/m^3)	2500
Friction Coefficient	0.2
Rolling friction coefficient	0
Restitution coefficient	0.2

4.4.2 Contact friction calibration

The model consists of a box with two halves, where the lower half is moved horizontally while the upper half remains fixed. All the walls, except the top one, were modeled as rigid boundaries (Figure 4.5). This rigid boundary condition does not have inertia and its velocity is imposed to control its position during the simulation. Walls interact with the particles, following the Hertz's contact model, to calculate the repulsive forces. The top boundary is modeled as a servo-controlled wall, in which its speed is related to the current stress.

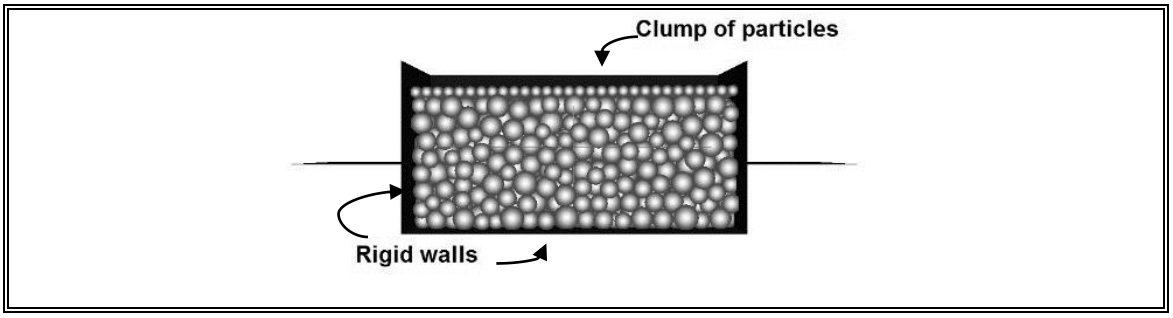

Figure 4.5: Direct Shear test DEM model used for contact friction calibration

The model is separated into two stages. The first consists in the creation of an assembly of 790 particles with the properties listed in Table 4.4; in this part of the model the contact friction has to be minimal to reach the void ratio required. Particularly the void ratio obtained for the model with null friction and gravity conditions was 0.658, which is reasonably similar to the laboratory set-up with void ratio 0.655 for G1.

In the second stage, the contact friction is increased in order to evaluate the soil response; no void ratio evolution is obtained in this stage. Confinement of 100 kPa is applied in the top wall, and after reaching static equilibrium, a displacement is applied in the lower half of the box.

Several tests were performed at confinement pressures of 50 and 100 kPa (three replications were performed at each confinement); results showed that a friction coefficient of 0.2 between particles gives a better stress-displacement response compared

with experimental data (Figure 4.6). The friction between particles and walls is assumed to be zero.

DEM simulation satisfactorily reproduces initial stiffness and its reduction with horizontal displacement, as well as the limit shear stress. Nevertheless, results show oscillations because the mean size of the grains is about 1/5 of the height of the sample (24 mm), hence macroscopic stresses are highly sensitive to any change in the force network because of the low number of contacts. This problem is avoided in the TS DEM model because the relation between the particle mean size and shortest dimension of the sample is less than 1/10.

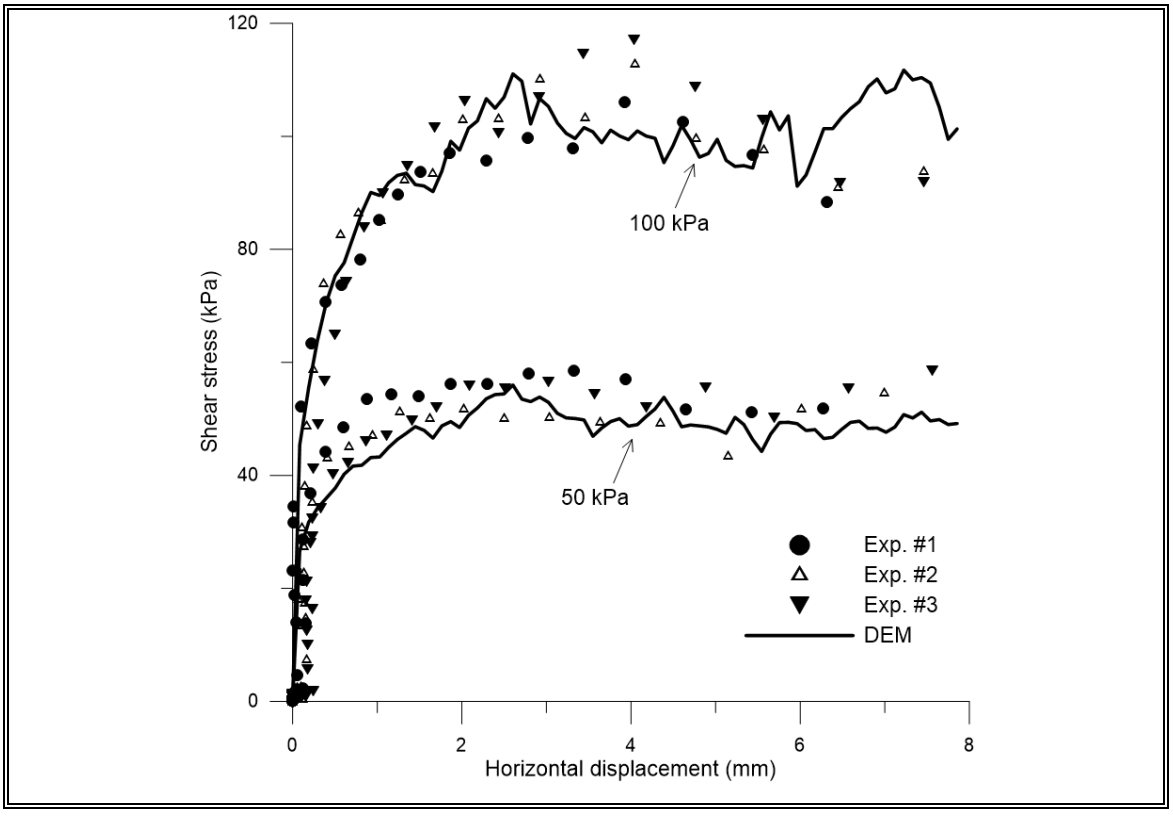

Figure 4.6: Stress displacement curve from experimental and simulated Direct Shear test

4.5 Torsional Shear DEM Model

4.5.1 Model setup

This model was developed in four phases in order to reduce computational effort and to make the iteration process easier since it is not necessary to run the entire model to make torsional loading modifications. Indeed, the torsion is the most critical phase since it was necessary to iterate in order to calibrate parameters and readjust the model; this is why this phase was isolated as the last one.

A rigid wall mesh cylinder shape was created to contain the assembly of 5100 (G1) and 33000 (G2) particles (Figure 4.7a). The dimensions of this cylinder are the same as the metal case used to build laboratory soil samples: 15 cm tall and 5 cm diameter. The wall mesh is also useful for further analysis since it can be used to measure its reaction forces. The number of particles was chosen accordingly for the target relative density of 40%. Similar to the preliminary direct shear test, if the friction coefficient is set to zero, a void ratio of 0.653 and 0.547 are obtained for G1 and G2, respectively, which is reasonably similar to the value used for the sample preparation at the laboratory. A null uniform inter-particle friction coefficient is used in the initial stage of the simulation to minimize the variation of initial porosity and avoid consolidation effects.

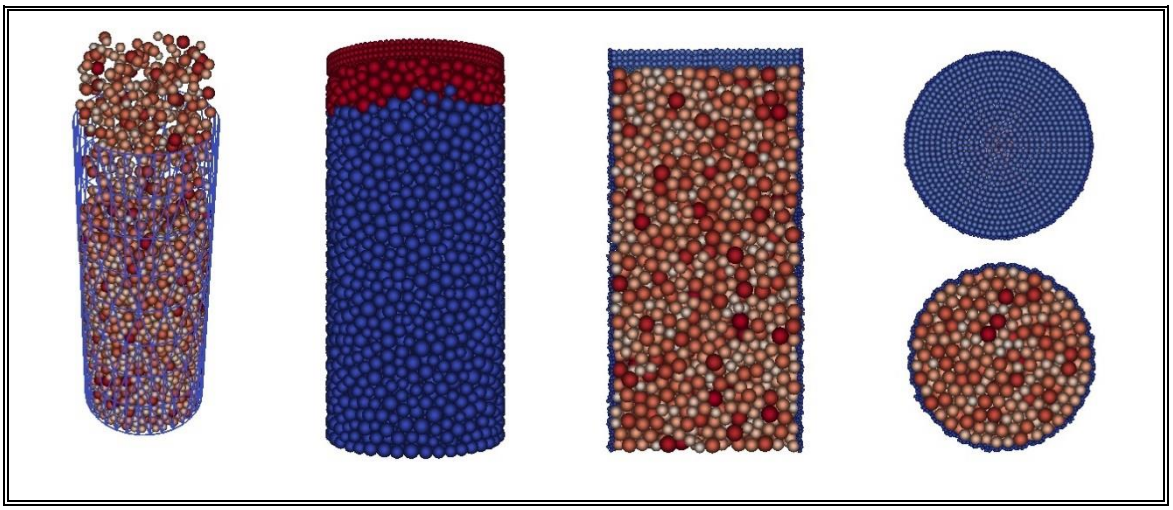

(a) (b) (c) (d)

Figure 4.7: DEM model phases: (a) sample creation inside cylindrical rigid wall, (b) clump casting and axial confinement, (c) membrane creation and isotropic confinement, (d) specimen plan view from top and bottom

4.5.2 Particles creation

In this stage, the capability of the model to represent the effects of the self-weight was evaluated. Particle stress (σ_{ij}^{p}) was calculated from contact forces (f_j^c) in direction from the particle p to centroid to contact point c over the particle volume (V_p).

$$\sigma_{ij}^{p} = \frac{1}{V_p}\sum_{c=1}^{N^{c,p}} |x_i^c - x_i^p| n_i^{c,p} f_j^c \qquad (4.3)$$

Where $|x_i^c - x_i^p|$ is the distance from the contact point (x_i^c) to the center of the particle (x_i^p), representing the radius in spherical particles.

The Figure 4.8 shows the distribution of vertical stress in the sample. Figure 4.8b compares geostatic vertical stress calculated from the experimental sample density versus the local vertical mean stress ($\bar{\sigma}_{ij} = \bar{\sigma}_{zz}$) calculated from particle stresses σ_{zz}^{p}. For this calculation the method proposed by Potyondy and Cundall [11] was used, which considers an adjustment of the measured volume (V) by the sample porosity (n).

$$\bar{\sigma}_{ij} = \frac{1}{V}\sum_{p=1}^{N_p} \sigma_{ij}^{p} V_p \qquad (4.4)$$

$$V = \frac{\sum_{p=1}^{N_p} V_p}{1-n} \qquad (4.5)$$

To define the measured volume we took a vertical slice of 6 mm thick across the vertical axis of the sample, then the slice was vertically divided into 10 rectangular strips of 10 mm tall and 50 m width. All particles with centroids within the volume were considered as a whole in this calculation. Finally the mean vertical stress $\bar{\sigma}_{zz}$ was obtained for each measured volume. Figures 4.8a and 8b show the force contact networks with line thicknesses proportional to their force amplitudes. Only normal forces exist in these cases since there is no friction between particles. The effect of gravity becomes evident as the contact forces' amplitudes increase with their depth. According to Figure 4.8b, mean stress is very close to the geostatic theoretical values, especially for the non-uniform G2 grading distribution. In the case of G1, some oscillations can be noted at the mid- portion of the sample that could be related to strong inclined contact forces as depicted in Figure 4.8a. These oscillations tend to vanish as the coordination number increases and the force network becomes more redundant, as can be noted from Figure 4.8c. Of course, contact forces' magnitudes are smaller for G2 because similar self-weight is transmitted across a large number of particles.

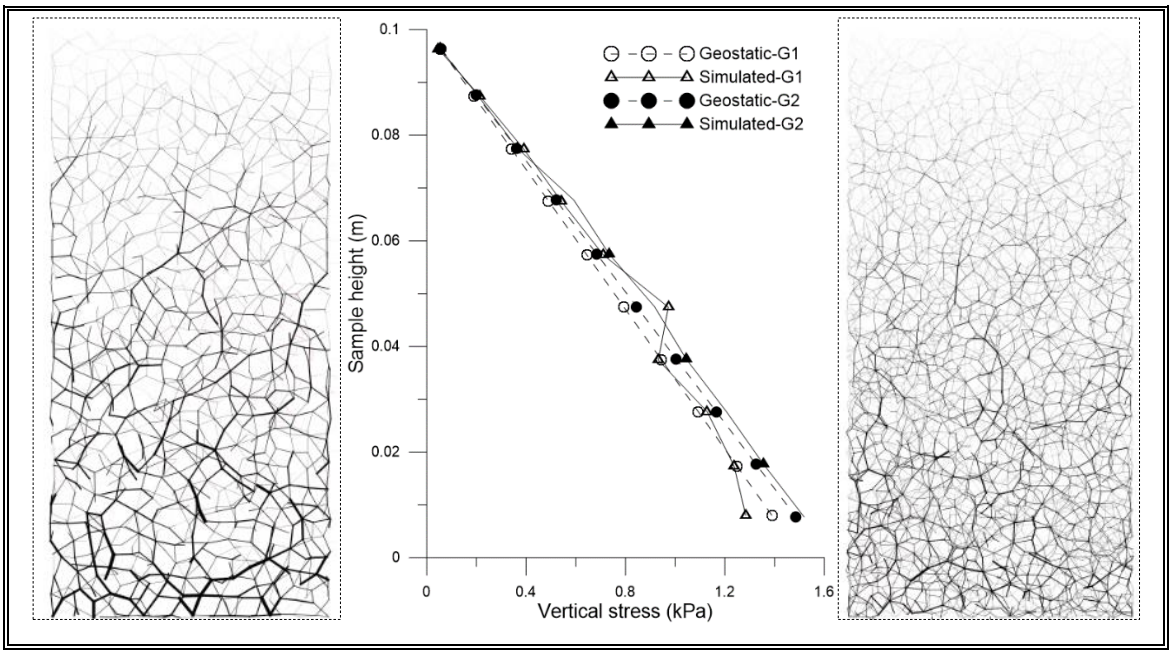

(a) (b) (c)

Figure 4.8: Stress distribution after model creation: (a) force network for G1 sample, (b) mean vertical stress distribution, (c) force network for G2 sample.

4.5.3 Initial confinement and clump casting

A rigid clump made out of spherical particles of 1 mm diameter was created at the top of the sample. The structure of this body was assembled by 3 layers of spheres, each one consisting of concentric rings of varying diameter from 23.5 to 1 mm (Figure 4.7d). As a result, we obtained an object composed of 3 discs, one on top of another, each one with 16 rings of particles varying in number according to each ring perimeter. In total the rigid clump has 2442 particles that work as a solid, continuous and rigid object. The clump particles have the same mechanical properties as the soil; they only differ from its density. The clump density was set up in order to replicate the real actuator's weight.

After the rigid mass is cast, the model runs until it reaches static equilibrium. Finally a uniaxial compression force is applied in each particle of the rigid body simulating the uniaxial compression pressure of 100kPa.

Additionally, in this stage of the model the particles at the top of the sample are gathered together with the rigid clump. Additionally, in this stage of the model, the

particles at the top of the sample are gathered together with the rigid clump; these particles at the top 10% of the same are equivalent to the 510 (G1) and 3000 (G2) beads. This strategy is applied to give mechanical interlock between the soil and the actuator (Figure 4.7b).

4.5.4 Membrane replacement strategy

With the aim of replicating laboratory conditions, it is imperative to allow the correct confinement pressure to be applied while allowing free deformation. Thus, a flexible membrane model was designed which consists in a cylindrical array of particles in which each atom is tethered to its initial position by a spring force. This allows keeping the overall shape of the membrane while giving it an elastic deformation feature controlled by a spring constant. At each time step, the magnitude of the tethering force on each atom is $-K\,r$, where r is the displacement of the atom from its current position to its initial position and K is a spring constant to be calibrated. It is important to mention that since the membrane particles are not bonded, they do not transmit moment, giving the membrane flexibility.

The membrane particles are hexagonally arranged and the initial position for each atom is calculated accordingly to an external cylinder shape of 25 mm radius and 110 mm height, which coats the rigid wall surface. The overall membrane consists in a 110 ring layers with 154 particles each totaling 16,940 particles (Figure 4.7c). For the uniform case, the size of each particle was chosen according to the criteria used by de Bono [4] which estimates the membrane particles should be 33% smaller than the smallest particle of soil. In the case of G2, the membrane particle size is about 90% of minimum particle size of the sample. The properties of each membrane particle are listed in Table 4.5.

Table 4.5 properties of modeled membrane

Property	Value
Density: γ (kg/m^3)	1000
Number of particles	16940
Spring stiffness: (N/m)	100
Frictional coefficient: μ (-)	0
Particle size: (mm)	1.0

At this stage no forces are applied to the membrane, and the rigid wall is still containing the soil. The next step will be removing the rigid wall and adding an equivalent force to the membrane to contain the soil with a 100kPa confinement.

4.5.5 Confinement

The last stage of the model has the objective of applying the confinement of the soil sample and then performing the torsional shear test by applying a cyclic angular displacement of the clump and attached soil portion. Both of those loading protocols are detailed next.

At this point, the soil sample is contained by a rigid wall mesh and a 100kPa pressure is applied on the top. In order to apply a confinement pressure of 100kPa, the rigid wall mesh has to be deactivated at the same time a force is applied to each particle of the membrane with direction pointing to the center of the cylinder shaped membrane. The compressed membrane encloses and covers the entire soil sample, as shown in Figure 4.7d.

The Figure 4.9 shows the contact network and mean stress distribution along the soil sample once external additional force was applied in the radial axis. It can be seen that the mean stress is reasonably close to the imposed value of 100 kPa. Similarly, as observed for the sample creation phase, the uniform particle size case (G1) shows an erratic stress distribution compared to the G2 sample. Additionally, mean stress values

tend to be larger than 100 kPa for G1, whereas they are in the range of 90 to 100 kPa for G2. Some confinement fluctuations could be related to the membrane particles, because in some parts of the G1 sample, particles go inside the DEM model because their sizes are comparable to the porosity and no bonding exits between them. This effect is also present at a minor scale in the G2 sample. Fluctuations in G1 tend to be higher because it has a lower number of particles. This means that there are discrete concentrations of forces, which influences the mean stress calculation within the measured volume.

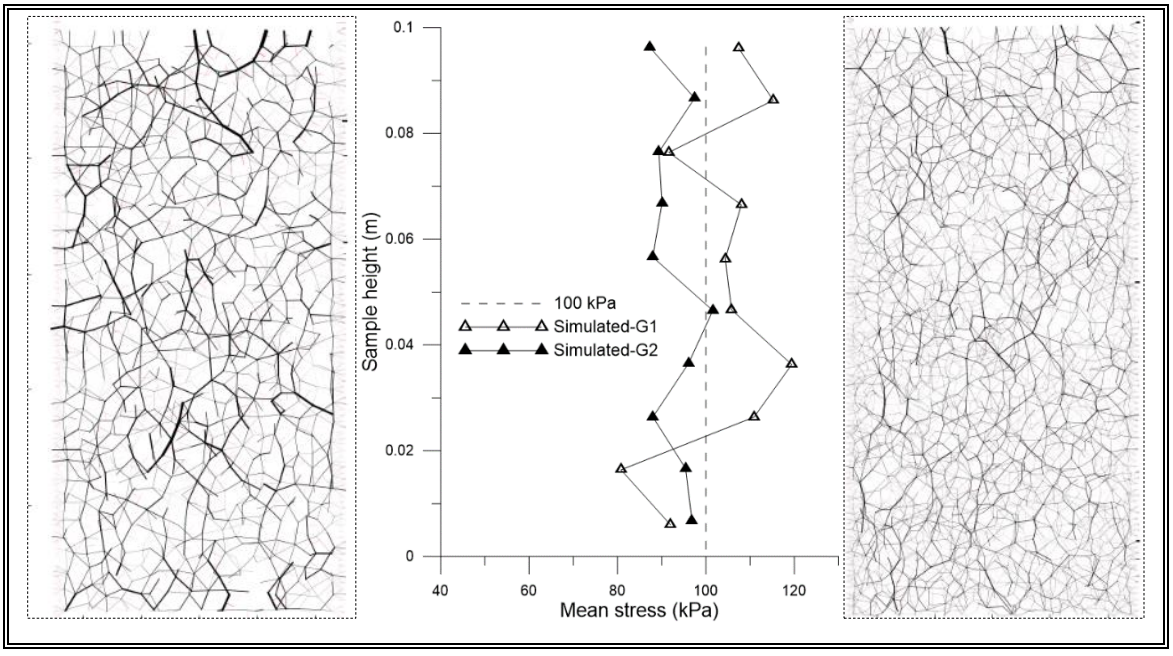

(a) (b) (c)

Figure 4.9: Stress distribution after membrane creation and confinement application: (a) force network for G1 sample, (b) mean stress distribution, (c) force network for G2 sample.

4.5.6 Cyclic angular distortion

To simulate the applied torsion, there are two options: doing it by controlling force or displacement. The first can be done by applying a torque, which is the way the laboratory test actually works. The second option consists in applying a top cap rotation.

Applying torque to a group of particles is not an available option in the free version of LIGGGHTS code, so we decided to simulate the torsional shear test controlling the angular displacement of the soil particles in the top of the sample.

First an angular motion was applied to the rigid clump, but the results were not satisfactory. The shear stress transfer was not properly simulated in this case since the contact surface between the rigid clump and soil particles did not have enough friction to prevent sliding in the interface. Even though we tried to increase contact friction and rolling friction between the actuator and the soil sample, it was not possible to simulate the necessary granular interlock to achieve the shear stress transfer.

Then, we used the soil itself to apply the sample rotation. It was not necessary to calibrate friction parameters between the soil and the rigid clump; the granular interlock gives enough strength to transfer shear stress. To properly distribute this rotation to the sample, all the particles over 0.08 m height were gathered into a group (top 10% of the soil sample), then the rotation was applied to all of them. These particles are represented by a red band in the Figure 4.7b.

Since the cyclic loading was applied due to angular deformation, the shearing velocity was controlled through the twist angle $\theta(t)$ which was described as a sinusoidal function in order to avoid any inertia effect on the resulting hysteresis loop when rotation sense changes. The applied twist velocity was controlled to minimize the effects of kinetic energy on the simulated G and D values. The angular distortion is defined by the amplitude θ_0 and the rate of rotation (frequency $f = 0.1\ Hz$), hence the computational time (t_0) necessary to reach the maximum required rotation is:

$$t_0 = \frac{\theta_0}{2\pi f} \qquad (4.6)$$

Once the twist angle is defined, the corresponding angular distortion is calculated from the top of the sample with the Eq. 4.2. The output of the model will be a calculated torque (T) using the sum of torque contribution from each soil particle in the red band (see Figure 4.7b) which had contact with any other particle from the rest of the soil sample.

Then the shear stress was calculated from Eq. 4.7, where r and J_p are the current radius and polar moment of inertia of the specimen.

$$\tau = \frac{rT}{J_p} \qquad (4.7)$$

4.6 DEM Model against experimental data

A series of fifteen simulations at $f = 0.1$ Hz were performed to assess the effect of degradation and loading conditions on material response.

4.6.1 Stiffness degradation and damping increase curves

For the current Cyclic Torsional Shear test study, a comparison of the macro-scale response observed in a laboratory test and the DEM simulation for the uniform and non-uniform specimen is illustrated in Figure 4.10. Stiffness degradation is shown as a normalized value by its maximum shear modulus. For the uniform DEM model, the lower strain level reached was 3×10^{-4} % where G_{max} reaches a value of 160 MPa while laboratory results show a G_{max} equal to 130 MPa at 1.5×10^{-4} %. This explains the difference in magnitude of the two curves presented in the Figure 4.10. In the case of G2, a G_{max} equal to 170 MPa at 3×10^{-4} % was obtained from the DEM model, while the experimental G_{max} was equal to 154 MPa at 1.5×10^{-4} %. Despite these differences, G1 degradation and the damping curve from DEM were very close to the experimental results across the explored strain range. In the case of G2, DEM models sub-estimate degradation for strain below 3×10^{-3} %, and overestimate degradation for strain larger than 2×10^{-2} %. For the non-uniform case, damping is sub-estimated for strains larger than 2×10^{-3} % but tendency is correctly reproduced.

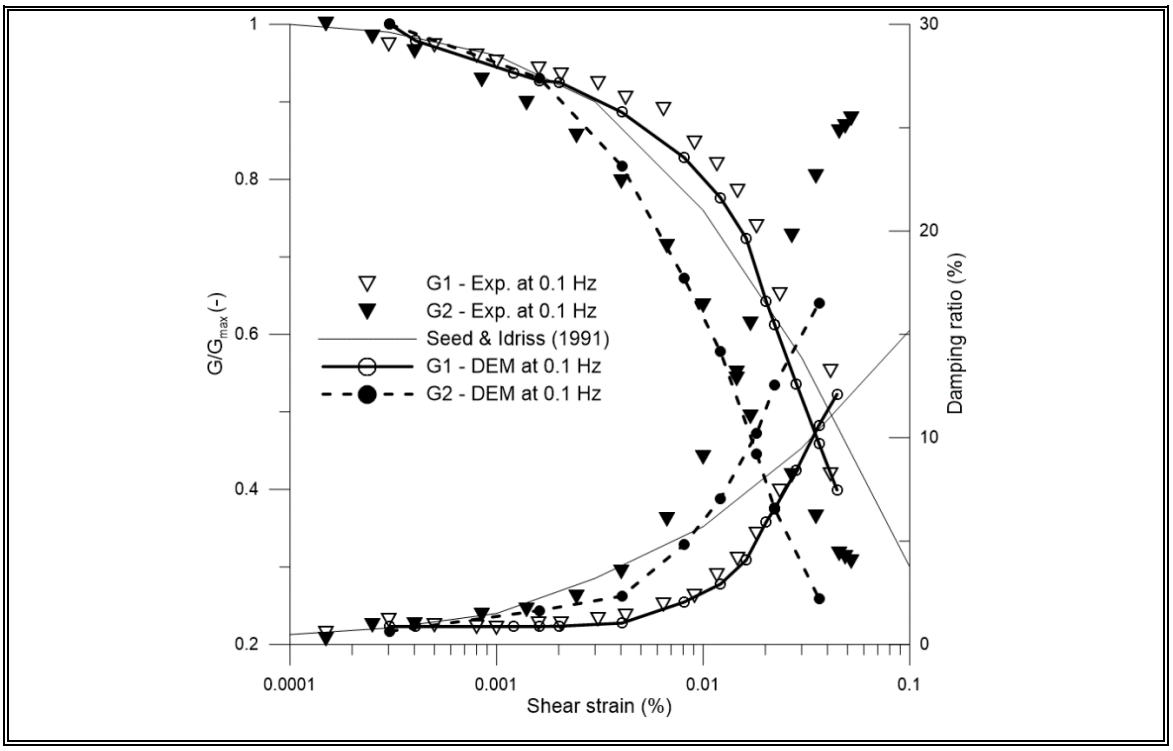

Figure 4.10: experimental and DEM stiffness degradation and damping curves for both particle size distributions

Even though the laboratory results show reasonable similar values for damping and shear modulus for low strains, Figure 4.11a shows that the hysteresis loop associated with low strains is not stable. This behavior tends to occur when imposed force magnitude is comparable with static contact forces. Thus, the software calculation at low deformations is adjusted to the cloud of points obtained. Regarding the DEM model at low strains, an unstable result can be seen but it is still possible to estimate a tendency for shear modulus calculation, while damping cannot be properly calculated. Therefore we decided to present the damping ratio results starting from 4×10^{-3} % strain. The damping values presented in Figure 4.10 below that deformation were replicated from this value.

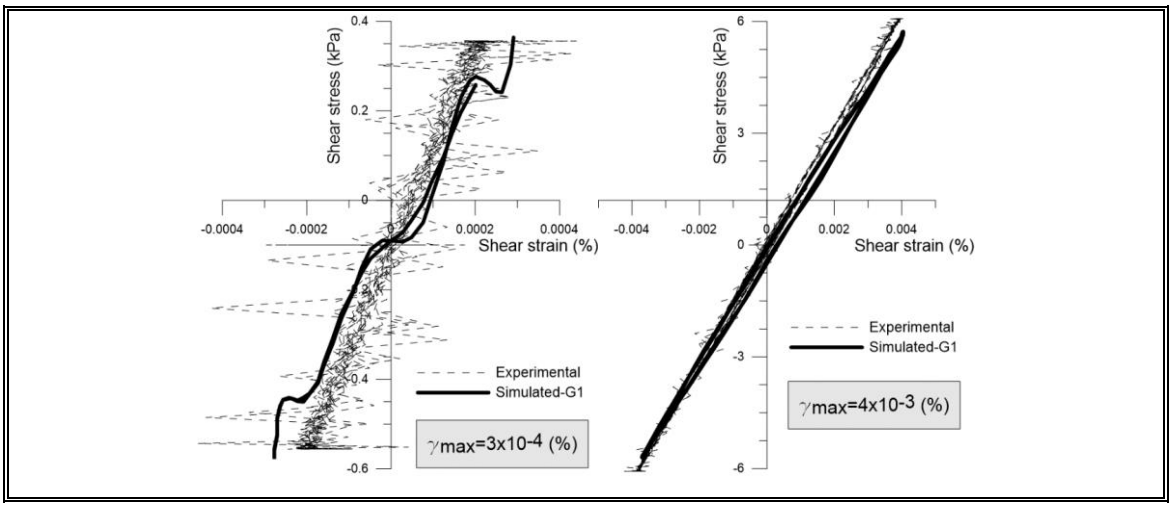

(a) (b)

Figure 4.11 experimental and simulated hysteresis loops at low strain levels. G1 uniform particle size distribution

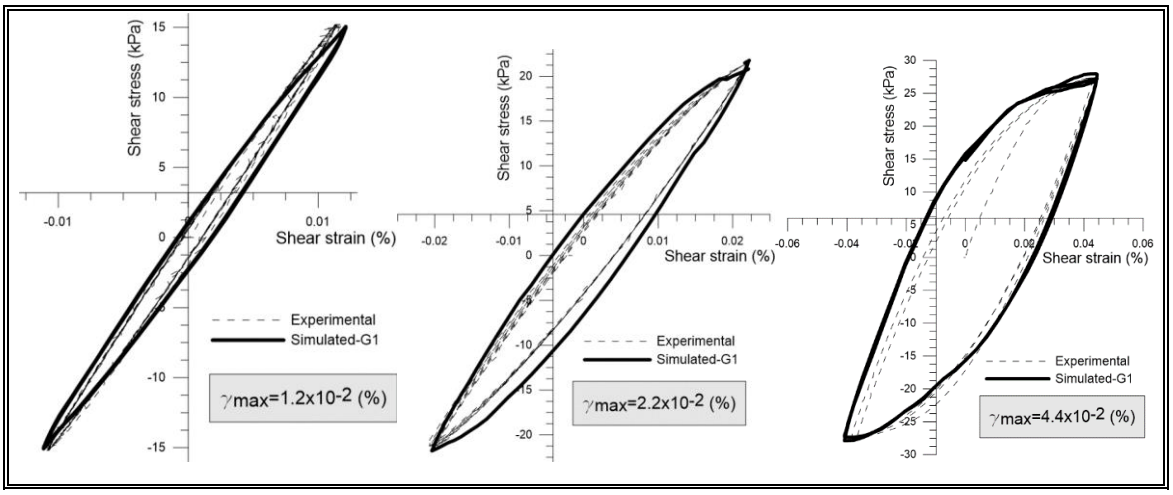

(a) (b) (c)

Figure 4.12: experimental and simulated hysteresis loops at different strain levels. G1 uniform particle size distribution

For higher strains, the match between laboratory and DEM hysteresis loops are very accurate since the laboratory results tend to stabilize and hysteresis loops become clear. The inclination of the DEM hysteresis loops tends to be smaller than the laboratory

test (Figure 4.11b), giving a lower shear modulus while the damping ratio shows very accurate results in medium strains (Figure 4.11c).

The highest angular distortion (γ_{max}) reached by the laboratory test was 0.044% (Figure 4.11e). At this range of strains observed residual deformations were observed; then we decided to use the first two hysteresis loops in order to compare with the DEM model.

4.6.2 Stress and strain distribution

As was mentioned before, a shear stress calculation of 0.8 times the radius ($r = 0.8R$) in order to have a representative shear strain for a given specimen. Thus, the distribution of torque was studied in the plane in which clumped particles transfer the shear stress to the soil (Figure 4.12). The torque at a fixed radius r for a selected maximum shear strain γ_{max} can be obtained as the integration of the corresponding circumferential shear stress $\tau_{z\theta}$ in cylindrical coordinates in a continuum sense or by the summation of horizontal amplitude of contact forces f_h^c located at a radius r_c smaller than r multiplied by its effective arm r_{arm}^c from the axisymmetric axis of the sample (Eq. 4.8). As previously indicated, only soil particles in contact with particles from the red band in Figure 4.7b are considered for this computation.

$$T(r, \gamma_{max}) = 2\pi \int_0^r \tilde{r}^2 \, \tau_{z\theta}(\tilde{r}, \gamma_{max}) \, d\tilde{r} \approx \sum_c^{r_c<r} r_{arm}^c \, f_h^c(\gamma_{max}) \tag{4.8}$$

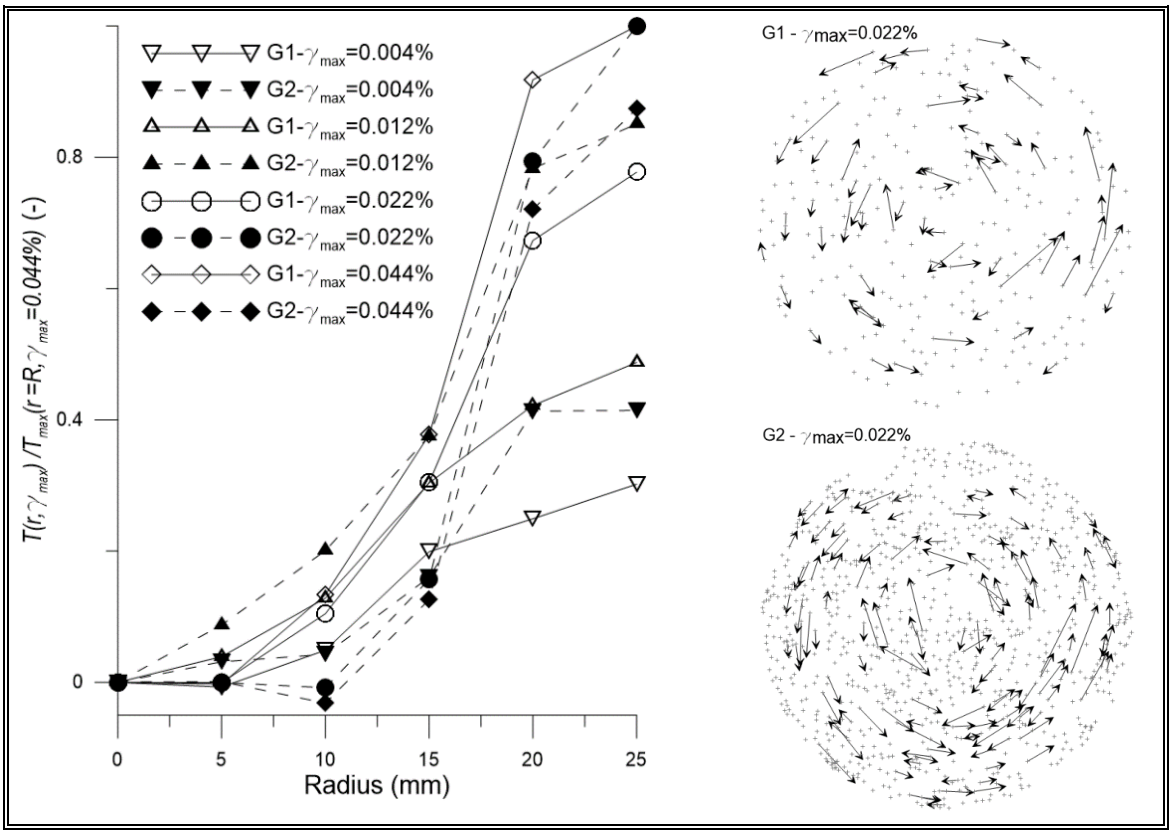

Figure 4.13: Shear load transfer micromechanics during TS test: (a) distribution of cumulated torque from axisymmetric axis of the sample; (b) and (c) 80% greatest horizontal contact forces at a maximum strain amplitude of $\boldsymbol{\gamma_{max}} = \mathbf{0.022}\%$ for G1 and G2 samples, respectively.

Figure 4.13a displays the values of torque $T(r, \gamma_{max})$ normalized by the maximum value computed for each sample, i.e. $T(r = R, \gamma_{max} = 0.044\%)$. In the case of the G1 sample, torque increase with the radius is monotonic and tends to an asymptotic value for $r > 20$ mm. In the case of G2, torque values are very low and erratic below $r < 10$ mm, and drastically increase for a radius larger than this value and become approximately stable for $r > 20$ mm. Moreover, G2 results at low strain (γ_{max} of 0.004% and 0.012%) show a similar distribution compared to the tendency obtained for the G1 sample. Indeed, distribution of larger explored shear strains (γ_{max} of 0.022% and 0.044%) are associated with a small negative value of cumulated torque at $r = 10$ mm, probably because at this level of strain some particle sliding and packing redistribution (or macroscopic inelastic behavior) takes place at weak contacts, inducing a more complex contact force

distribution. Figures 4.12b and 4.12c display horizontal components of contact forces at a maximum shear strain of $\gamma_{max} = 0.022\%$ for G1 and G2 samples, respectively. Only 80% of the greatest forces have been displayed in these figures to simplify the presentation (all contacts positions are indicated by gray crosses). According to Figure 4.12b, almost all forces are counter-clockwise oriented inducing a monotonous increase of cumulated torque from the center of the sample in the G1 case. In contrast, the orientation of horizontal forces is erratic for the G2 case close to the center, explaining oscillations of cumulated torque for $r < 10$ mm. For larger distances from the center of the sample, counter-clockwise orientation of forces predominates stabilizing the increase of cumulated torque in the sample.

In summary, despite complex torque distribution close to the central sample axis highlighted for some cases, results show that at 0.8 times radius, i.e. at 20 mm from the central axis of the specimen, the cumulative torque reaches approximately 90% of the total torque applied to the soil sample at the current level of applied maximum strain. So it can be concluded that this assumption represents a satisfactory approach in terms of shear stress transfer representativeness.

To explore the shear strain distribution in the torsional shear specimen, Figure 4.14 shows the twist angle and shear strain evolution against sample height using both G1 and G2 samples. It can be seen that for both samples with different coordination numbers, the behavior of the specimen rotation along the sample tends to be linear for strains lower than 0.004% (Figure 4.14a). While deformation increases, the motion transfer from the top to the bottom of the sample decreases, since intergranular sliding starts occur exhibiting a non-linear behavior. In fact, macroscopic damping increases drastically for strains larger than about 0.004%. This effect is most evident in G2 where contact forces are weaker.

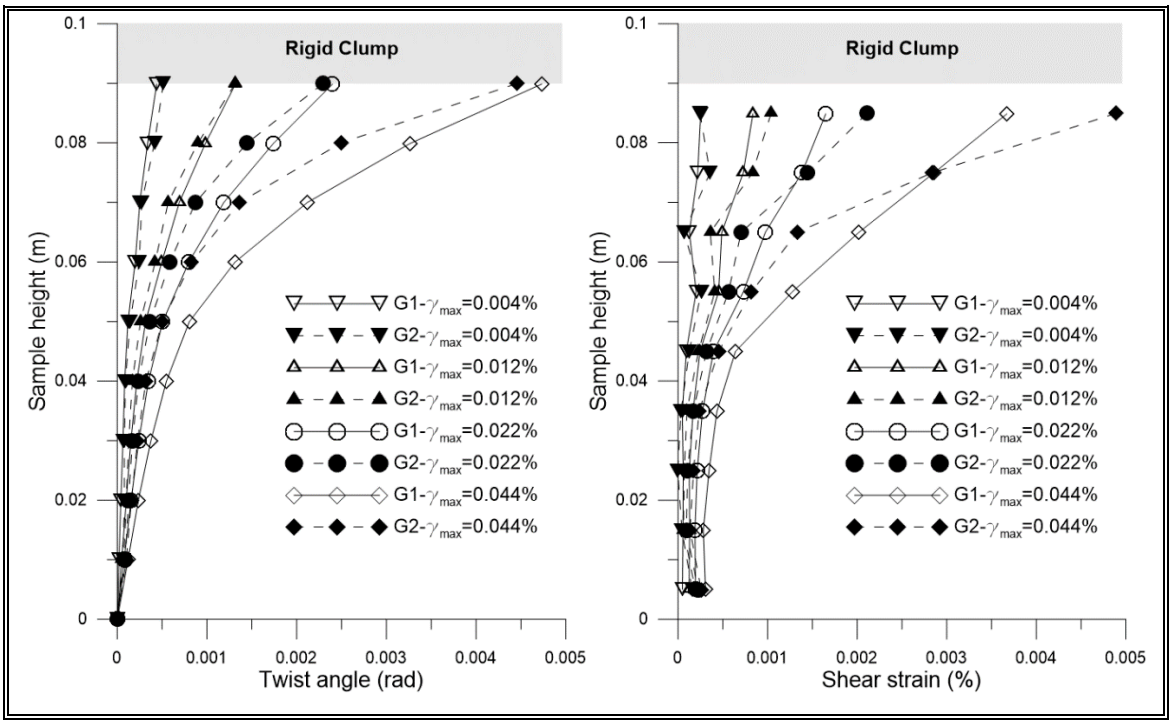

(a) (b)

Figure 4.14: distribution of twist angle and shear strain in simulated samples.

Regarding the shear strain along the sample height, it is observed that the uniform sample has a smoother transition in deformations from the top to its base (Figure 4.14b), while the sample with a higher coordination number shows bigger differences in strain per each section measured. Moreover, we observed the twist band to be approximately 1/2 of the sample height in the case of the uniform sample while the non-uniform sample was only 1/3 of its height.

4.7 Conclusions

A DEM model has been created that successfully reproduces the Cyclic Torsional Shear test on a granular media made out of glass beads for two different grain size distributions. The results presented in the work show that the discrete model could properly replicate the macroscopic experimental stress strain behavior from laboratory tests.

The sample force network and calculated mean stress shows that the modeled membrane satisfactorily reproduced the confinement effect. Some confinement fluctuations could be related to displacement of membrane particles inside the DEM model because their sizes are comparable to the porosity and no bonding exits between them. As the sample coordination number increases, this effect is reduced because a large number of particles is included in the control volume used to calculate mean stresses. Indeed, oscillation of mean stress is reduced with a greater coordination number because the force network becomes more homogenous.

To apply the torsional excitation to the soil sample, an angular displacement is imposed on the soil particles in the top of the specimen in addition to the rigid clump. This strategy promotes shear stress transfer by granular interlock between soil particles and also avoids the calibration process between the actuator and the soil sample. To properly reproduce imposed torque using angular displacement, it is necessary to control the shearing velocity in order to avoid any inertia effect on the resulting hysteresis loop when the rotation sense changes.

The match between laboratory and DEM resulting shear strain curves are very accurate as the laboratory results tend to stabilize and hysteresis loops becomes clear. In general, the inclination of the DEM hysteresis loops tend to be smaller than the laboratory test sub-estimating shear modulus, while damping results are very close to laboratory results for G1, but not so in G2 where damping is underestimated.

The simulated *G* degradation and *D* increase curves derived from the resulting hysteresis loops are compared with laboratory tests in a resulting degradation curve from 10^{-4} % to 4×10^{-2} % strain. Thus, the DEM model is able to replicate the experimental data not only in a similar trend but also in a very close magnitude. Uniform sample degradation and damping curve represent better experimental adjustment than a non-uniform sample.

A linear behavior of the strain distribution within the specimen is observed for small deformations. As the deformation increases, the motion transfer from the top to the bottom of the sample decreases probably because sliding starts to occur, exhibiting a

macroscopic non-linear behavior. This effect is manifested most while the coordination number increases and contact forces become weaker in average.

Despite complex torque distribution close to the central sample axis that was highlighted in some cases, results show that at 0.8 times radius the cumulative torque reaches approximately 90% of the total torque applied. So it can be concluded that this assumption represents a satisfactory approach in terms of shear stress transfer representativeness. DEM simulations also indicate the formation of twist band in approximately 1/2 of the sample height in the case of the uniform sample while the non-uniform sample at only 1/3 of its height.

Acknowledgments

This work was made possible by a grant from the Chilean National Commission for Scientific and Technological Research under FONDEQUIP Award Number EQM120061 and was partially supported by the National Research Center for Integrated Natural Disaster Management CONICYT/ FONDAP/15110017.

References

[1] American Society for Testing and Materials. (2007). Standard Test Methods for Modulus and Damping of Soils by Resonant-Column Method. *ASTM Standard D 4015-07*, *92*(Reapproved 2000), 1–22. http://doi.org/10.1520/D4015-07.1.3.2

[2] Assimaki, B. D., Kausel, E., & Whittle, A. (2000). Model for dynamic shear modulus and damping for granular soils. *Journal of Geotechnical and Environmental Engineering*, 859–869. http://doi.org/10.1061/(ASCE)1090-0241(2000)126:10(859)

[3] Boltachev, G. S., Volkov, N. B., & Zubarev, N. M. (2012). Tangential interaction of elastic spherical particles in contact. *International Journal of Solids and Structures*, *49*(15-16), 2107–2114. http://doi.org/10.1016/j.ijsolstr.2012.04.013

[4] Bono, J., Mcdowell, G. & Wanatowski, D. (2012). Discrete element modelling of a flexible membrane for triaxial testing of granular material at high pressures.

Géotechnique Letters, *2*(October-December), 199–203. http://doi.org/10.1680/geolett.12.00040

[5] Cui, L., & O'sullivan, C. (2006). Exploring the macro-and micro-scale response of an idealized granular material in the direct shear apparatus. *Geotechnique*, 56(7), 455–468. http://dx.doi.org/10.1680/geot.2006.56.7.455

[6] Cundall, P., & Strack, O. (1979). A discrete numerical model for granular assemblies. *Geotechnique*, 29(1), 47–65.

[7] El Mohtar, C. S., Drnevich, V. P., Santagata, M., & Bobet, A. (2013). Combined Resonant Column and Cyclic Triaxial Tests for Measuring Undrained Shear Modulus Reduction of Sand With Plastic Fines. *Geotechnical Testing Journal*, *36*(4), 20120129. http://doi.org/10.1520/GTJ20120129

[8] Ishihara, K. (1996). *Soil Behaviour in Earthquake Geotechnics*. New York: Oxford University Press.

[9] Li, Y., Xu, Y., & Thornton, C. (2005). A comparison of discrete element simulations and experiments for sandpiles composed of spherical particles. *Powder Technology*, 160(3), 219– 228. http://doi.org/10.1016/j.powtec.2005.09.002

[10] Li, B., Zhang, F., & Gutierrez, M. (2014). Numerical DEM Examination of a Torsional Shear Test. *Geo-Congress 2014 Technical Papers*, 2887–2897. http://doi.org/10.1061/9780784413272.280

[11] Masson, S. & Martinez, J. (2001). Micromechanical analysis of the shear behavior of a granular material. *Journal of engineering mechanics*, 127(10), 1007–1016. http://dx.doi.org/10.1061/(ASCE)0733-9399(2001)127:10(1007)

[12] O'Donovan, J., O'Sullivan, C., Marketos, G., & Muir Wood, D. (2015). Analysis of bender element test interpretation using the discrete element method. *Granular Matter*, *17*(2), 197–216. http://doi.org/10.1007/s10035-015-0552-6

[13] O'Sulivan, C. (2011). Particle-based discrete element modeling: Geomechanics perspective. International Journal of Geomechanics. 449–464. http://doi.org/10.1061/(ASCE)GM.1943-5622.0000024

[14] O'Sullivan, C., Cui, L., and O'Neill, S. C. (2008). Discrete element analysis of the response of granular materials during cyclic loading. *Soils Found*. 48(4), 511–530. http://doi.org/10.3208/sandf.48.511

[15] O'Sullivan, C. (2015). Advancing geomechanics using DEM, 21–32. K. Soga (2015) *Geomechanics from micro to macro.* London: Taylor & Francis Group.

[16] O'Sullivan, C. (2011). *Particulate discrete element modeling*. New York: Routledge.

[17] Padilla, J.M. (2004). *GCTS Resonant Column Device*. GCTS Testing systems.

[18] Ravichandran, N., Machmer, B., Krishnapillai, H., & Meguro, K. (2010). Micro-scale modeling of saturated sandy soil behavior subjected to cyclic loading. *Soil Dynamics and Earthquake Engineering*, *30*(11), 1212–1225. http://doi.org/10.1016/j.soildyn.2010.05.002

[19] Salazar, A., Sáez, E., & Pardo, G. (2014). Modeling the direct shear test of a coarse sand using the 3d Discrete ElementMethod with a rolling friction model. *Submitted to Computers and Geotechnique*. http://doi.org/10.1016/j.compgeo.2015.02.017

[20] Suzuki, K., & Kuhn, M. R. (2013). Discrete Element Simulations of Cyclic Biaxial Shear of a Granular Material with Oval Particles. *International Journal of Geomechanics*, 1–8. http://doi.org/10.1061/(ASCE)GM.1943-5622.0000328.

[21] Tallavo, F., Cascante, G., Asce, M., Sadhu, A., Asce, A. M., & Pandey, M. D. (2014). New Analysis Methodology for Dynamic Soil Characterization Using Free-Decay Response in Resonant-Column Testing. *Journal of Geotechnical an Environmental Engineering*, 121–132. http://doi.org/10.1061/(ASCE)GT.1943-5606.0000984.

[22] Tong, L., & Wang, Y. H. (2014). DEM simulations of shear modulus and damping ratio of sand with emphasis on the effects of particle number, particle shape, and aging. *Acta Geotechnica*, *10*(1), 117–130. http://doi.org/10.1007/s11440-014-0331-2

[23] Towhata, I. (2008). *Geotechnical Earthquake Engineering*. Berlin: Springer.

[24] Yan, Y., & Ji, S. (2010). Discrete element modeling of direct shear tests for a granular material. *International journal for numerical and analytical methods in geomechanics*, 34(9), 978–990. http://doi.org/10.1002/nag.848

[25] Zhao, X., Evans, T. M., & Asce, A. M. (2010). Discrete Simulations of Laboratory Loading Conditions. International Journal of Geomechanics, 169–178. http://doi.org/10.61/(ASCE)532-3641(2009)9:4(169)

5. CONCLUSIONS

A DEM model has been created that successfully reproduces the Cyclic Torsional Shear test on a granular media made out of glass beads for two different grain size distributions. This numerical simulations not only monitor the global mechanical response but also examine the micromechanics response which may improve the understanding the physics of particle systems.

Model results shows the simulated loading protocol can properly reproduce macroscopic response of the synthetic material for both particle size distribution. The sample force network and calculated mean stress shows that the confinement effect is satisfactorily applied by the modeled membrane. Regarding the torsional excitation, it is imposed an angular displacement to the soil particles in the top of the specimen in addition to the rigid clump. This strategy promotes shear stress transfer by granular interlock between soil particles and also avoids the calibration process between the actuator and the soil sample. For properly reproduce imposed torque using angular displacement it is necessary to control the shearing velocity in order to avoid any inertia effect on the resulting hysteresis loop when rotation sense changes.

The global stress strain behavior observed in the numerical model can properly replicate the real response of measured data from laboratory tests. The simulated G degradation and D increase curves are derived from the resulting hysteresis loop obtained from both model and experimental data. Both cases are compared in the resulting degradation curve at different strain levels, which replicates the experimental data not only in a similar trend but also in a very close magnitude.

At a micro-mechanical level it is observed a homogenization of the force network as the particle coordination number increases. This homogenization of contact forces leads to decreasing contact normal forces at the weak contacts. Hence, particle sliding becomes easier to occur at those weak contacts in the non-uniform sample than in the uniform sample, and therefore, the damping ratio is increased. Regarding the strain level along the sample height, it is observed that the uniform sample has a smoother transition in deformations from the top to its base, while the sample with higher coordination number

shows bigger differences in strain per each section measured. Moreover, the twist band it is observed to be 1/2 of the sample height in the case of the uniform sample while the non-uniform sample only 1/3 of its height.

With the results presented in this paper arises the discussion of which is the strain level to which the soil specimen is being subjected during the cyclic torsional shear test, since the theoretical linear strain distribution do not properly reproduces the soil behavior for deformations over 10^{-4} %. As the real shear strain observed in the model is less than idealized, the values of *G* and *D* are probably lower (higher for *D*) to those reported traditionally given a level of deformation.

5.1 Further work

In this study it is built a degradation curve at a limited deformations range. Then, referring to the strain levels studied it might be considered a simulation of different laboratory test such as cyclic triaxial or hollow cylinder test. Figure 5.11 illustrates the strain range covered by multiple laboratory tests.

An important point to consider when exploring larger deformations, is that volume changes and pore pressure variations might occur. Then, coupling the water to the problem becomes important. Particularly, it would be necessary to include computational fluid dynamics coupling if it is wanted to explore a range of major deformations for general saturated case.

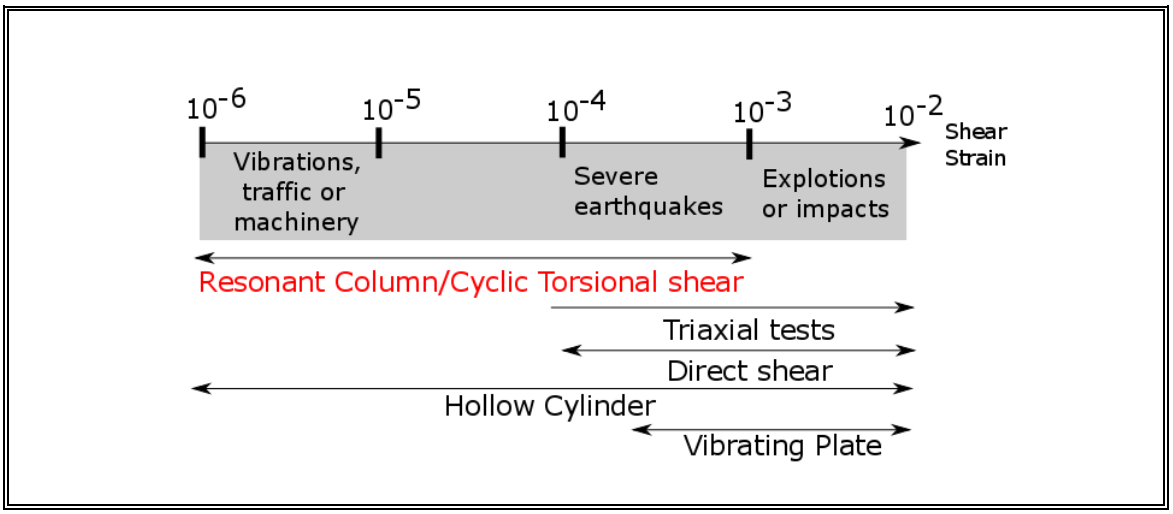

Figure 5.1: shear strain range for commonly used laboratory tests (modified from Sáez, 2016).

Regarding to the tested material, the future investigations might consider the use of another material, such as oval particle shape or a real coarse sand. Using this simulations it could be included the effect of the shape of grains with different methods, other rolling frictions models, or clumps methodologies. The latter is probably the most advanced of all, in which it is used a multi-sphere model to replicate irregular particle shapes.

While the materials discussed in this work attempt to model a sand at the grain scale, clay or silt is more difficult to model due to the large difference in scale. This will mean that the number of particles simulated will limit the computational feasibility for solving the model. Therefore the simulations can rather attempt to reproduce the micro-mechanical processes at the scale of the sand grains using soil bulk properties. In addition, other considerations should be taken into account for fine soil modelling such as water interaction, particle bonding and loading frequency dependency.

REFERENCES

American Society for Testing and Materials. (2007). Standard Test Methods for Modulus and Damping of Soils by Resonant-Column Method. *ASTM Standard D 4015-07*, *92*(Reapproved 2000), 1–22. http://doi.org/10.1520/D4015-07.1.3.2

Assimaki, B. D., Kausel, E., & Whittle, A. (2000). Model for dynamic shear modulus and damping for granular soils. *Journal of Geotechnical and Environmental Engineering*, 859–869.

Boltachev, G. S., Volkov, N. B., & Zubarev, N. M. (2012). Tangential interaction of elastic spherical particles in contact. *International Journal of Solids and Structures*, *49*(15-16), 2107–2114. http://doi.org/10.1016/j.ijsolstr.2012.04.013

Ci, L., & O'sullivan, C. (2006). Exploring the macro-and micro-scale response of an idealized granular material in the direct shear apparatus. *Geotechnique*, 56(7), 455–468.

Cundall, P., & Strack, O. (1979). A discrete numerical model for granular assemblies. *Geotechnique*, 29(1), 47–65.

El Mohtar, C. S., Drnevich, V. P., Santagata, M., & Bobet, A. (2013). Combined Resonant Column and Cyclic Triaxial Tests for Measuring Undrained Shear Modulus Reduction of Sand With Plastic Fines. *Geotechnical Testing Journal*, *36*(4), 20120129. http://doi.org/10.1520/GTJ20120129

Ishihara, K. (1996). *Soil Behaviour in Earthquake Geotechnics*. New York: Oxford University Press.

Li, Y., Xu, Y., & Thornton, C. (2005). A comparison of discrete element simulations and experiments for sandpiles composed of spherical particles. *Powder Technology*, 160(3), 219– 228.

Li, B., Zhang, F., & Gutierrez, M. (2014). Numerical DEM Examination of a Torsional Shear Test. *Geo-Congress 2014 Technical Papers*, 2887–2897. http://doi.org/10.1061/9780784413272.280

Masson, S. & Martinez, J. (2001). Micromechanical analysis of the shear behavior of a granular material. *Journal of engineering mechanics*, 127(10), 1007–1016.

Mcdowell, G., Wanatowski, D., & de Bono, J. (2012). Discrete element modelling of a flexible membrane for triaxial testing of granular material at high pressures. *Géotechnique Letters*, *2*(October-December), 199–203. http://doi.org/10.1680/geolett.12.00040

O'Donovan, J., O'Sullivan, C., Marketos, G., & Muir Wood, D. (2015). Analysis of bender element test interpretation using the discrete element method. *Granular Matter*, *17*(2), 197–216. http://doi.org/10.1007/s10035-015-0552-6

O'Sulivan, C. (2011). Particle-based discrete element modeling: Geomechanics perspective. International Journal of Geomechanics. 449–464. http://doi.org/10.1061/(ASCE)GM.1943-5622.0000024

O'Sullivan, C., Cui, L., and O'Neill, S. C. (2008). Discrete element analysis of the response of granular materials during cyclic loading. *Soils Found*. 48(4), 511–530.

O'Sullivan, C. (2015). Advancing geomechanics using DEM, 21–32. K. Soga (2015) *Geomechanics from micro to macro.* London: Taylor & Francis Group.

O'Sullivan, C. (2011). *Particulate discrete element modeling*. New York: Routledge.

Padilla, J.M. (2004). GCTS Resonant Column Device.

Ravichandran, N., Machmer, B., Krishnapillai, H., & Meguro, K. (2010). Micro-scale modeling of saturated sandy soil behavior subjected to cyclic loading. *Soil Dynamics and Earthquake Engineering*, *30*(11), 1212–1225. http://doi.org/10.1016/j.soildyn.2010.05.002

Salazar, A., Sáez, E., & Pardo, G. (2014). Modeling the direct shear test of a coarse sand using the 3d Discrete ElementMethod with a rolling friction model. *Submitted to Computers and Geotechnique.*

Sáez, E. (2016). Three problems and their three modeling scales in Soil Dynamics. *Personal communication.*

Suzuki, K., & Kuhn, M. R. (2013). Discrete Element Simulations of Cyclic Biaxial Shear of a Granular Material with Oval Particles. *International Journal of Geomechanics*, 1–8. http://doi.org/10.1061/(ASCE)GM.1943-5622.0000328.

Tallavo, F., Cascante, G., Asce, M., Sadhu, A., Asce, A. M., & Pandey, M. D. (2014). New Analysis Methodology for Dynamic Soil Characterization Using Free-Decay Response in Resonant-Column Testing. *Journal of Geotechnical an Environmental Engineering*, 121–132. http://doi.org/10.1061/(ASCE)GT.1943-5606.0000984.

Tong, L., & Wang, Y. H. (2014). DEM simulations of shear modulus and damping ratio of sand with emphasis on the effects of particle number, particle shape, and aging. *Acta Geotechnica*, *10*(1), 117–130. http://doi.org/10.1007/s11440-014-0331-2

Towhata, I. (2008). *Geotechnical Earthquake Engineering*. Berlin: Springer.

Yan, Y., & Ji, S. (2010). Discrete element modeling of direct shear tests for a granular material. *International journal for numerical and analytical methods in geomechanics*, 34(9), 978–990.

Zhao, X., Evans, T. M., & Asce, A. M. (2010). Discrete Simulations of Laboratory Loading Conditions. International Journal of Geomechanics, 169–178. http://doi.org/10.61/(ASCE)532-3641(2009)9:4(169)

APENDIX

A. EXPERIMENTAL RESULTS

A.1 Resonant column test of G1 sample at 100 kPa

Sample : RC1-100-01
Water condition : Saturated
Particle size distribution : G1
Confinement pressure : 100 (KPa)

Gamma [%]	Damping Ratio	G [Mpa]	G/G0
0.0149	5.827	115.59	0.78222914
0.01447	4.146	115.54	0.78189078
0.01301	3.369	119.608	0.80942005
0.01059	2.527	123.772	0.83759897
0.00708	1.489	130.1	0.88042228
0.00603	1.393	132.24	0.89490424
0.00492	1.146	134.34	0.90911552
0.00299	1.3	136.583	0.94429451
0.00126	1.321	143.185	0.96897205
0.001	1.473	143.165	0.96883671
0.00065	1.302	145.409	0.98402247
0.0004	1.2	145.48	0.98450294
0.00021	1.21	145.408	0.9840157
0.00021	1.235	145.445	0.98426609
0.00016	1.18	147.77	1

Sample : RC1-100-02
Water condition : Saturated
Particle size distribution : G1
Confinement pressure : 100 (KPa)

Gamma [%]	Damping Ratio	G [Mpa]	G/G0
0.01531	5.474	115.584	0.79218854
0.01525	4.781	113.525	0.77825472
0.01393	3.561	115.528	0.79180957
0.01152	2.787	119.583	0.81925086
0.00747	1.618	125.813	0.86141098
0.0066	1.514	125.811	0.87139744
0.00533	1.284	129.967	0.89952223
0.0031	1.2	132.186	0.91453881
0.00129	1.199	134.36	0.92925086
0.00106	0.919	136.511	0.93380727
0.00078	1.116	136.459	0.93345537
0.00051	1.56	138.669	0.94841104
0.00026	1.078	143.133	0.97862015
0.0002	1.5	140.903	0.96352913
0.00018	1.542	140.962	0.9639284
0.00014	1.4	138.73	0.94882385

Sample : RC1-100-03
Water condition : Saturated
Particle size distribution : G1
Confinement pressure : 100 (KPa)

Gamma [%]	Damping Ratio	G [Mpa]	G/G0
0.02117	4.1	109.59	0.80314545
0.01007	3.8	119.627	0.87670299
0.00825	2.397	122.607	0.89854233
0.00588	2.366	123.73	0.90677239
0.00485	2.195	125.81	0.92201596
0.00388	1.576	127.95	0.93769925
0.00244	1.391	127.95	0.93769925
0.00129	1.189	132.187	0.96875069
0.00073	0.979	134.325	0.98441932
0.00023	0.796	136.451	1

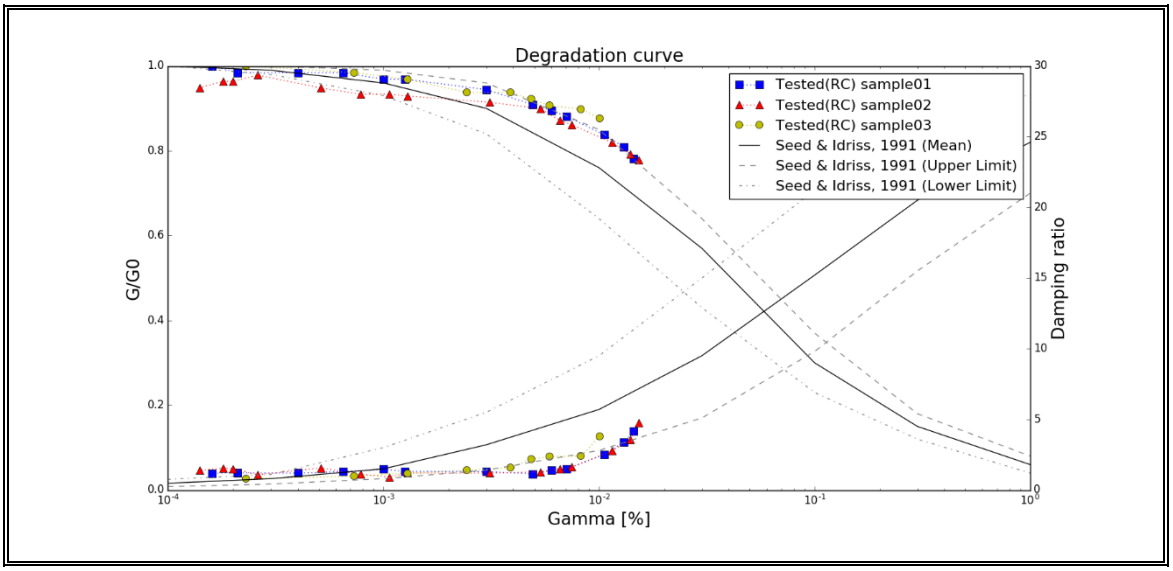

A.2 Resonant column test of G1 sample at 200 kPa

Sample : RC1-200-01
Water condition : Saturated
Particle size distribution : G1
Confinement pressure : 200 (KPa)

Gamma [%]	Damping Ratio	G [Mpa]	G/G0
0.01981	3.03	171.213	0.85914935
0.01307	1.645	176.332	0.88483656
0.01228	1.561	178.74	0.89691994
0.00805	1.16	181.288	0.90970584
0.00459	0.936	183.76	0.92211038
0.00457	1.233	186.41	0.93540812
0.00353	1.124	183.855	0.92258709
0.00332	1.336	181.24	0.90946498
0.00194	1.316	186.464	0.93567909
0.00192	1.19	183.78	0.92221074
0.00129	1.169	194.055	0.97377084
0.00115	1.249	188.982	0.94831445
0.00072	1.471	191.496	0.96092974
0.00064	1.095	196.684	0.9869632
0.00061	1.4	188.965	0.94822914
0.00018	1.149	199.282	1

Sample : RC1-200-02
Water condition : Saturated
Particle size distribution : G1
Confinement pressure : 200 (KPa)

Gamma [%]	Damping Ratio	G [Mpa]	G/G0
0.01371	2.858	164.044	0.85992714
0.01197	2.779	159.364	0.83539433
0.00988	1.821	169.059	0.88621603
0.00803	1.639	169.028	0.88605352
0.00661	1.146	171.654	0.89981915
0.00524	1.253	171.712	0.90012319
0.00398	1.285	176.914	0.92739234
0.00311	1.366	177.35	0.92967788
0.00098	1.156	185.061	0.97009934
0.00079	1.721	187.703	0.98394884
0.00057	0.879	190.362	0.99788745
0.00019	1.503	188.069	0.98586743
0.00013	1	190.765	1

Sample : RC1-200-03
Water condition : Saturated
Particle size distribution : G1
Confinement pressure : 200 (KPa)

Gamma [%]	Damping Ratio	G [Mpa]	G/G0
0.01599	3.743	166.427	0.84646997
0.01522	2.777	166.395	0.84630721
0.01388	1.977	168.81	0.85859023
0.01109	1.853	171.296	0.87123435
0.00715	1.529	176.121	0.89577495
0.00618	1.441	178.72	0.90899381
0.005	1.267	181.191	0.92156165
0.00288	1.129	183.678	0.93421086
0.00112	0.888	188.747	0.95999247
0.00092	0.949	188.83	0.96041462
0.00062	1.325	191.393	0.97345038
0.00043	1.157	193.969	0.98655226
0.00018	1	193.979	0.98660312
0.00019	1.28	196.589	0.99987793
0.00012	1	196.613	1

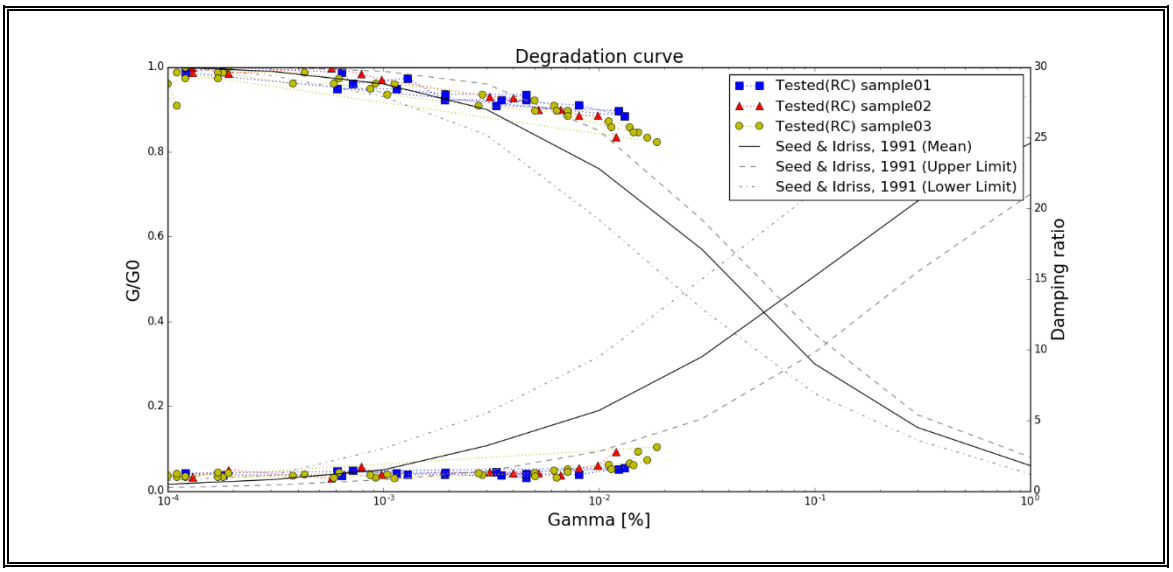

A.3 Cyclic torsional shear test of G1 sample at 100 kPa

Sample : TS1-100-01
Water condition : Saturated
Particle size distribution : G1
Confinement pressure : 100 (KPa)
Frequency : 0.1 (Hz)

Gamma [%]	Damping Ratio	G [Mpa]	G/G0
0.00015	0.5483	128.63	1
0.0003	1.1586	125.26	0.97380082
0.0005	0.934	125.15	0.97294566
0.0008	0.8554	123.44	0.95965171
0.001	0.8144	122.43	0.95179974
0.0016	0.9879	121.21	0.94231517
0.00205	1.0157	120.3	0.93524061
0.0031	1.2278	118.89	0.92427894
0.0042	1.3927	116.43	0.90515432
0.00645	1.9188	114.56	0.8906165
0.00905	2.3511	108.95	0.84700303
0.01165	3.3511	105.34	0.81893804
0.0146	4.144	100.92	0.78457592
0.0181	5.324	95.11	0.7394076
0.02345	7.405	83.79	0.65140325
0.0412	13.209	53.92	0.41918682

Sample : TS1-100-01
Water condition : Saturated
Particle size distribution : G1
Confinement pressure : 100 (KPa)
Frequency : 0.2 (Hz)

Gamma [%]	Damping Ratio	G [Mpa]	G/G0
0.0002	0.6652	126.83	1
0.00035	0.5372	125.05	0.98596547
0.0006	0.9626	122.63	0.96688481
0.00095	1.1465	122.16	0.96317906
0.0012	1.0351	121.27	0.95616179
0.00195	1.4637	119.95	0.94575416
0.00245	1.4899	118.92	0.93763305
0.00365	1.5023	119.36	0.94110226
0.00495	1.7157	117.02	0.92265237
0.0076	2.1192	114.2	0.90041788
0.01045	2.7091	111.03	0.8754238
0.0135	3.8149	107.45	0.84719704
0.0168	4.4149	103.75	0.81802413
0.0206	5.9589	98.52	0.77678783
0.0259	9.3897	89.67	0.70700938

Sample : TS1-100-01
Water condition : Saturated
Particle size distribution : G1
Confinement pressure : 100 (KPa)
Frequency : 0.5 (Hz)

Gamma [%]	Damping Ratio	G [Mpa]	G/G0
0.0001	0.607	134.74	1
0.0002	0.1985	130.48	0.96838355
0.00035	0.8811	129.26	0.95932908
0.0006	1.0084	127.57	0.9467864
0.001	1.0475	126.79	0.94099748
0.00125	0.9643	126.9	0.94181386
0.00205	1.3343	125.11	0.92852902
0.00255	1.3269	124.07	0.92081045
0.0039	1.6428	121.95	0.90507644
0.00535	1.8453	118.75	0.881327
0.00825	2.5136	115.32	0.85587057
0.01135	3.051	111.72	0.82915244
0.01465	3.795	108.05	0.8019148
0.0183	4.7634	103.75	0.77000148
0.0223	5.6762	99.48	0.73831082
0.0281	9.2092	90.21	0.66951165
0.0419	12	68.04	0.50497254

Sample : TS1-100-01
Water condition : Saturated
Particle size distribution : G1
Confinement pressure : 100 (KPa)
Frequency : 1 (Hz)

Gamma [%]	Damping Ratio	G [Mpa]	G/G0
0.0002	3.2232	136.43	1
0.00035	0.1085	131.16	0.96137213
0.0006	0.7269	127.91	0.93755039
0.00095	1.4613	126.39	0.92640915
0.0012	1.2676	124.85	0.91512131
0.00195	1.6103	123.45	0.90485964
0.0025	1.6674	121.44	0.89012681
0.0038	1.9709	119.82	0.87825258
0.0052	2.1801	116.59	0.85457744
0.0081	2.9581	112.94	0.82782379
0.01115	3.7299	108.96	0.79865132
0.01445	4.511	105.15	0.77072491
0.0181	5.6278	101.03	0.74052628
0.02215	7.1929	96.15	0.70475702
0.0276	10.1976	88.18	0.64633878

Sample : TS1-100-01
Water condition : Saturated
Particle size distribution : G1
Confinement pressure : 100 (KPa)
Frequency : 2 (Hz)

Gamma [%]	Damping Ratio	G [Mpa]	G/G0
0.0001	1.0423	135.79	1
0.0002	1.2529	131.36	0.9673761
0.00035	1.3421	129.32	0.9523529
0.0006	1.1056	128.91	0.94933353
0.001	1.4614	127.46	0.93865528
0.00125	1.8399	127.41	0.93828706
0.002	1.6798	125.72	0.92584137
0.00255	1.715	125.02	0.92068635
0.00385	2.0151	123.09	0.90647323
0.00525	2.2387	120.36	0.88636866
0.00815	2.7266	116.89	0.86081449
0.01115	3.2907	113.79	0.83798512
0.01435	3.9354	110.19	0.8114736
0.01785	4.7381	106.35	0.78319464
0.0218	5.9851	101.63	0.74843508
0.02725	8.9916	92.96	0.68458649
0.03895	13	73.24	0.53936225

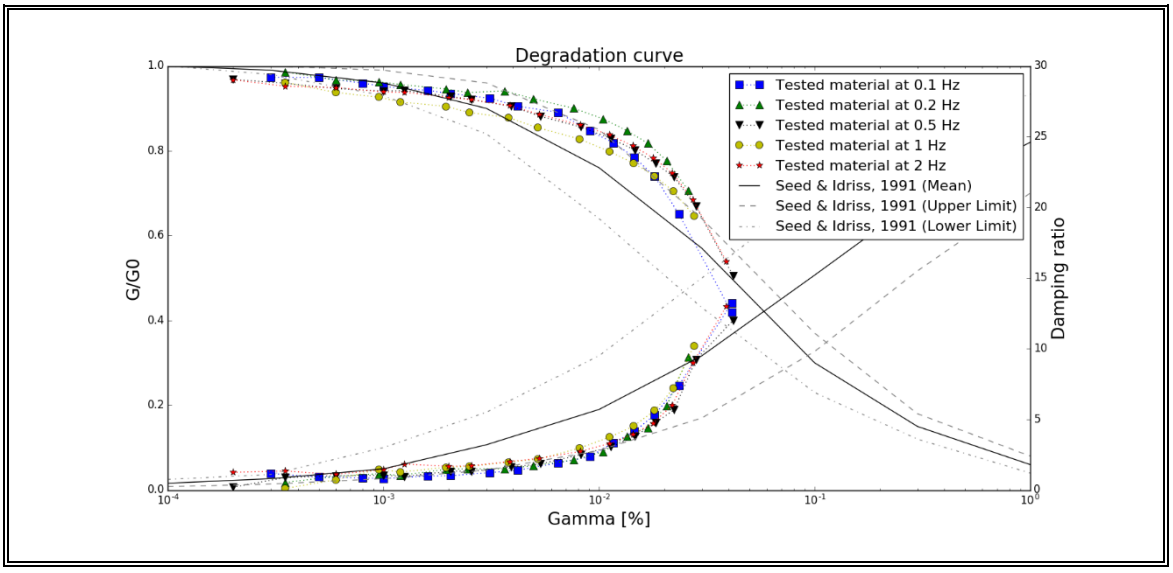

Sample : TS1-100-02
Water condition : Saturated
Particle size distribution : G1
Confinement pressure : 100 (KPa)
Frequency : 0.2 (Hz)

Gamma [%]	Damping Ratio	G [Mpa]	G/G0
0.00035	1.1732	198.76	1
0.00075	1.1629	192.63	0.96915878
0.0012	1.4055	191.18	0.96186355
0.0015	1.3517	190.51	0.95849265
0.0023	1.4319	188.86	0.95019119
0.0031	1.577	186.15	0.93655665
0.00475	1.8691	183.3	0.92221775
0.0064	2.2566	180.54	0.90833166
0.00815	2.4693	177.73	0.894194
0.00995	2.7053	174.63	0.8785973
0.0118	3.09	171.84	0.86456027
0.01375	3.8756	168.71	0.84881264
0.01595	5.0216	163.73	0.8237573
0.019	7.1883	152.44	0.76695512

Sample : TS1-100-02
Water condition : Saturated
Particle size distribution : G1
Confinement pressure : 100 (KPa)
Frequency : 0.5 (Hz)

Gamma [%]	Damping Ratio	G [Mpa]	G/G0
0.0001	1.71	214.69	1
0.00025	1.1109	210.3	0.97955191
0.0004	1.2372	209.9	0.97768876
0.0008	1.3483	202.93	0.94522335
0.00125	1.3439	201.39	0.93805021
0.0016	1.5659	199.33	0.92845498
0.0024	1.7286	198.78	0.92589315
0.0033	1.8562	192.22	0.89533746
0.00505	2.3304	188.3	0.87707858
0.00685	2.594	184.49	0.85933206
0.00875	2.9124	180.93	0.84275001
0.01075	3.2598	176.6	0.8225814
0.01275	3.4324	173.59	0.80856118
0.01495	3.8436	169.57	0.78983651
0.01745	4.7271	163.3	0.76063161
0.02095	6.52	151.33	0.7048768

Sample : TS1-100-02
Water condition : Saturated
Particle size distribution : G1
Confinement pressure : 100 (KPa)
Frequency : 1 (Hz)

Gamma [%]	Damping Ratio	G [Mpa]	G/G0
0.0002	2.0264	206.01	1
0.00035	1.6534	205.41	0.99708752
0.00075	1.1793	201.97	0.9803893
0.00125	1.5561	198.22	0.9621863
0.00155	1.6717	196.3	0.95286637
0.00235	1.882	194.12	0.94228436
0.0032	1.9707	190.98	0.92704238
0.0049	2.2766	186.97	0.9075773
0.0066	2.5473	183.83	0.89233532
0.00845	2.9248	179.86	0.87306441
0.01035	3.2094	175.97	0.85418184
0.01235	3.5829	172.3	0.83636717
0.01455	4.0934	167.15	0.81136838
0.0171	4.7717	160.15	0.77738945
0.0198	6.061	153.73	0.74622591

Sample : TS1-100-02
Water condition : Saturated
Particle size distribution : G1
Confinement pressure : 100 (KPa)
Frequency : 2 (Hz)

Gamma [%]	Damping Ratio	G [Mpa]	G/G0
0.0002	1.64	212.27	1
0.0004	1.7178	209.34	0.98619683
0.00075	1.8379	207.18	0.97602111
0.00125	2.0251	205.12	0.96631648
0.00155	1.9895	202.93	0.95599944
0.0024	2.14	200.13	0.94280869
0.00325	2.2647	196.27	0.9246243
0.00495	2.6289	191.44	0.90187026
0.00675	2.8912	187.46	0.88312055
0.00865	3.1805	183.5	0.86446507
0.01055	3.5543	179.87	0.84736421
0.0126	3.9326	175.73	0.82786074
0.0149	4.3777	170.05	0.80110237
0.0176	4.9218	161.92	0.76280209
0.021	6.4071	150.86	0.71069864

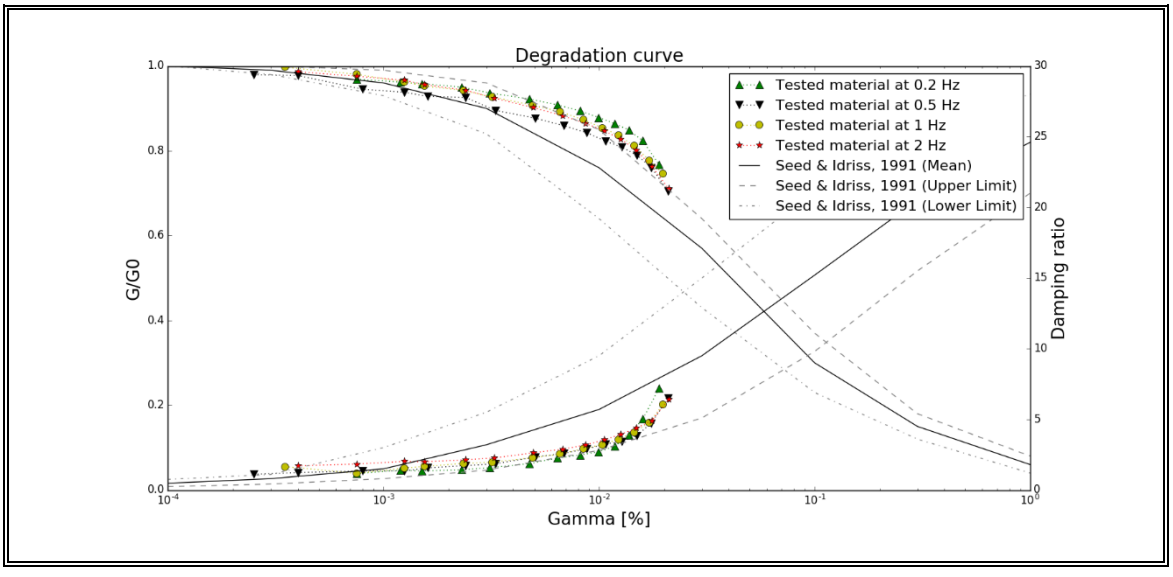

Sample : TS1-100-03
Water condition : Dry
Particle size distribution : G1
Confinement pressure : 100 (KPa)
Frequency : 0.2 (Hz)

Gamma [%]	Damping Ratio	G [Mpa]	G/G0
0.00005	0.17	186.95	1
0.00015	0.6651	182.83	0.97796202
0.00025	1.007	186.71	0.99871623
0.0004	1.3015	184.25	0.98555764
0.0008	1.151	181.29	0.96972453
0.0013	1.4057	178.25	0.95346349
0.00165	1.4699	177.04	0.94699117
0.0025	1.9321	174.63	0.93410003
0.0034	2.15	170.89	0.91409468
0.0052	2.54	167.21	0.89441027
0.00695	3.15	166.94	0.89296603
0.00905	4.98	160.21	0.8569671

Sample : TS1-100-03
Water condition : Dry
Particle size distribution : G1
Confinement pressure : 100 (KPa)
Frequency : 0.5 (Hz)

Gamma [%]	Damping Ratio	G [Mpa]	G/G0
0.0002	1.055	212.91	1
0.0004	1.3935	208.4	0.97881734
0.00075	1.2918	204.71	0.96148607
0.00125	1.5814	202.22	0.94979099
0.0016	1.5576	200.88	0.94349725
0.0024	1.71	198.67	0.93311728
0.0032	1.5748	197.25	0.9264478
0.00495	2.476	191.89	0.90127284
0.00685	3.0354	185.16	0.86966324
0.009	4.48	176.15	0.82734489
0.0116	6.78	163.79	0.76929219

Sample : TS1-100-03
Water condition : Dry
Particle size distribution : G1
Confinement pressure : 100 (KPa)
Frequency : 1 (Hz)

Gamma [%]	Damping Ratio	G [Mpa]	G/G0
0.00005	4.8	223.9	1
0.0001	2.0856	219.16	0.97882984
0.0002	2.0996	213.48	0.95346137
0.00035	1.7336	212.74	0.95015632
0.0007	1.7279	210.73	0.9411791
0.0012	1.9186	207.21	0.92545779
0.0015	1.7309	204.86	0.91496204
0.00225	1.9646	203.02	0.90674408
0.00305	2.0863	198.98	0.88870031
0.00465	2.0173	196.47	0.87748995
0.00635	2.7928	191.92	0.85716838
0.0082	3.84	185.88	0.83019205
0.01025	5.54	178.53	0.7973649

Sample : TS1-100-03
Water condition : Dry
Particle size distribution : G1
Confinement pressure : 100 (KPa)
Frequency : 2 (Hz)

Gamma [%]	Damping Ratio	G [Mpa]	G/G0
0.00005	0.6529	222.88	1
0.0001	1.9334	217.39	0.97536791
0.0002	1.3348	220.41	0.9889178
0.00035	2.1115	217.01	0.97366296
0.00075	2.0237	212.74	0.95450467
0.0012	2.069	210.03	0.94234566
0.0015	2.189	208.1	0.93368629
0.0023	2.2817	204.92	0.91941852
0.00315	2.46	200.36	0.89895908
0.00485	2.5	196.86	0.88325556
0.00655	2.873	193.62	0.86871859
0.0084	3.5522	188.78	0.84700287
0.0104	4.539	182.59	0.81923008
0.0127	5.858	174.71	0.78387473
0.0152	8.7	166.97	0.74914752

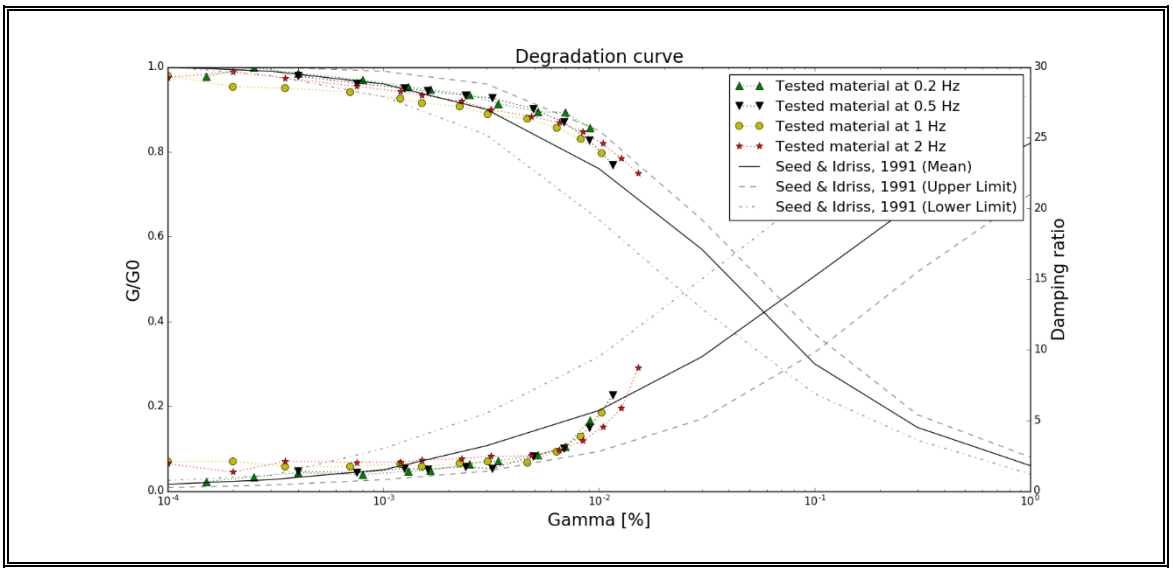

A.4 Cyclic torsional shear test of G1 sample at 200 kPa

Sample : TS1-200-01
Water condition : Saturated
Particle size distribution : G1
Confinement pressure : 200 (KPa)
Frequency : 0.1 (Hz)

Gamma [%]	Damping Ratio	G [Mpa]	G/G0
0.0002	0.6678	165.15	1
0.0004	0.877	163.98	0.99291553
0.0006	0.6569	162.7	0.985165
0.00075	0.849	162.89	0.98631547
0.0012	0.9172	161.61	0.97856494
0.00155	0.8645	161.01	0.97493188
0.0023	1.102	159.67	0.96681804
0.00315	1.1519	156.96	0.95040872
0.00475	1.3684	154.71	0.93678474
0.00645	1.4929	152.55	0.92370572
0.00815	1.6745	150.81	0.91316985
0.0099	1.8535	148.79	0.90093854
0.0117	2.0709	147.04	0.89034211
0.01355	2.3282	144.92	0.8775053
0.0155	2.7568	142.74	0.86430518
0.01775	3.7205	138.61	0.83929761

Sample : TS1-200-01
Water condition : Saturated
Particle size distribution : G1
Confinement pressure : 200 (KPa)
Frequency : 0.2 (Hz)

Gamma [%]	Damping Ratio	G [Mpa]	G/G0
0.00005	0.3031	170.53	1
0.00015	0.23	168.16	0.98610215
0.00025	0.2016	166.06	0.9737876
0.00045	1.1585	165.51	0.97056236
0.0007	0.6857	165.74	0.9719111
0.0009	0.7224	164.49	0.96458101
0.0014	0.9129	164.35	0.96376004
0.0018	0.8763	163.48	0.9586583
0.0027	1.0109	161.98	0.94986219
0.00365	1.1293	159.24	0.93379464
0.00555	1.3344	156.84	0.91972087
0.0075	1.4891	154.59	0.90652671
0.0095	1.684	152.53	0.89444673
0.01155	1.9085	150.57	0.88295315
0.0137	2.1962	148.45	0.87052132
0.01585	2.55	146.29	0.85785492
0.01815	3.0583	143.62	0.84219785
0.02095	4.4129	138.59	0.81270158

Sample : TS1-200-01
Water condition : Saturated
Particle size distribution : G1
Confinement pressure : 200 (KPa)
Frequency : 0.5 (Hz)

Gamma [%]	Damping Ratio	G [Mpa]	G/G0
0.00015	0.89	168.48	1
0.0003	0.2538	166.36	0.9874169
0.0005	0.9928	164.61	0.97702992
0.0008	0.7796	163.45	0.97014482
0.00095	0.5972	163.97	0.97323124
0.00155	0.9079	161.68	0.95963913
0.00195	0.9591	160.99	0.95554369
0.0033	1.1301	159.63	0.94747151
0.00405	1.1704	157.12	0.9325736
0.00615	1.4	154.78	0.91868471
0.0083	1.584	152.79	0.90687322
0.0105	1.6722	150.85	0.8953585
0.01275	1.8686	149.07	0.88479345
0.01505	2.0318	147.42	0.875
0.0174	2.2661	145.61	0.86425689
0.0198	2.5694	143.81	0.85357312
0.02265	3.529	139.67	0.82900048

Sample : TS1-200-01
Water condition : Saturated
Particle size distribution : G1
Confinement pressure : 200 (KPa)
Frequency : 1 (Hz)

Gamma [%]	Damping Ratio	G [Mpa]	G/G0
0.00045	0.6965	168.97	1
0.00075	0.7879	163.23	0.96602947
0.0009	1.0472	164.96	0.97626798
0.0015	1.2472	163.01	0.96472747
0.0019	1.1564	161.58	0.95626443
0.00285	1.2567	160.08	0.94738711
0.00385	1.3845	157.27	0.93075694
0.0059	1.5108	155.15	0.91821033
0.00795	1.6141	153.31	0.90732083
0.01005	1.8211	151.49	0.89654968
0.0122	1.9378	149.77	0.88637036
0.01435	2.0902	148.25	0.87737468
0.0166	2.3338	146.54	0.86725454
0.0189	2.6141	144.78	0.85683849
0.0215	3.2928	141.52	0.83754513

Sample : TS1-200-01
Water condition : Saturated
Particle size distribution : G1
Confinement pressure : 200 (KPa)
Frequency : 2 (Hz)

Gamma [%]	Damping Ratio	G [Mpa]	G/G0
0.00005	1.88	173.5	1
0.00015	1.7488	165.55	0.95417867
0.0003	1.6726	168.96	0.97383285
0.0005	1.2924	165.09	0.95152738
0.00075	1.341	165	0.95100865
0.00095	1.3953	164.75	0.94956772
0.00155	1.4977	163.5	0.94236311
0.00195	1.5604	161.89	0.93308357
0.003	1.6405	159.48	0.91919308
0.004	1.7578	157.8	0.90951009
0.0061	1.8518	155.7	0.89740634
0.00825	2.011	153.74	0.88610951
0.0104	2.1398	151.95	0.87579251
0.01265	2.2861	150.19	0.86564842
0.01495	2.6039	148.1	0.85360231
0.0173	3.1372	146.47	0.84420749
0.01965	2.9733	144.99	0.83567723
0.0223	3.5044	142.04	0.79560858

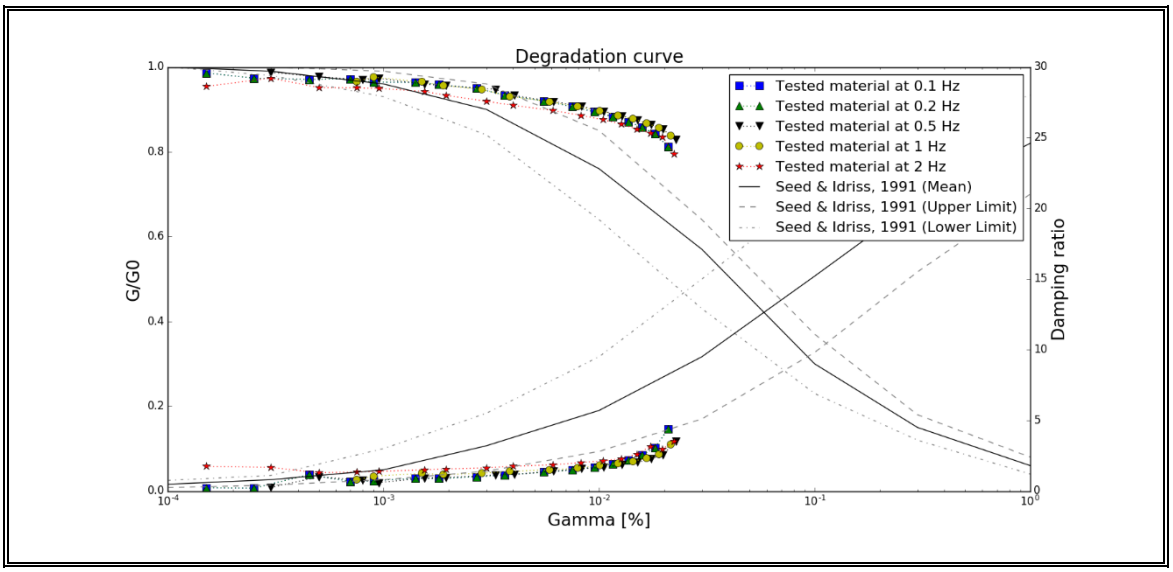

Sample : TS1-200-02
Water condition : Saturated
Particle size distribution : G1
Confinement pressure : 200 (KPa)
Frequency : 0.2 (Hz)

Gamma [%]	Damping Ratio	G [Mpa]	G/G0
0.0001	1.1887	287.12	1
0.00025	1.0882	284.51	0.99090972
0.0005	1.289	280.56	0.97715241
0.00085	1.088	278.49	0.96994288
0.00105	1.1375	278.03	0.96834076
0.0016	1.1703	275.51	0.95956395
0.00215	1.3523	271.98	0.94726943
0.00325	1.438	268.53	0.93525355
0.00435	1.5244	266.51	0.92821817
0.0055	1.6298	264.33	0.92062552
0.00665	1.7665	262	0.91251045
0.00785	1.9183	259.52	0.90387295
0.009	2.0449	257.69	0.8974993
0.0102	2.2387	255.59	0.89018529
0.01155	2.5011	251.38	0.87552243

Sample : TS1-200-02
Water condition : Saturated
Particle size distribution : G1
Confinement pressure : 200 (KPa)
Frequency : 0.5 (Hz)

Gamma [%]	Damping Ratio	G [Mpa]	G/G0
0.00025	0.8623	290.94	1
0.00055	1.3759	285.33	0.98071767
0.0009	1.2151	281.69	0.9682065
0.00115	1.2391	280.04	0.96253523
0.0017	1.45	277.91	0.95521413
0.0023	1.5351	273.24	0.93916271
0.0035	1.6501	269.85	0.92751083
0.00475	1.7083	266.93	0.91747439
0.006	1.7768	264.6	0.90946587
0.00725	1.8582	262.58	0.90252286
0.0085	1.9738	261.18	0.89771087
0.0098	2.0968	258.91	0.88990857
0.0111	2.2263	256.57	0.88186568
0.01255	2.4396	252.24	0.86698288

Sample : TS1-200-02
Water condition : Saturated
Particle size distribution : G1
Confinement pressure : 200 (KPa)
Frequency : 1 (Hz)

Gamma [%]	Damping Ratio	G [Mpa]	G/G0
0.00025	0.9772	285.57	1
0.00055	1.158	283.5	0.99275134
0.00085	1.3914	280.4	0.98189586
0.0011	1.5043	278.96	0.97685331
0.00165	1.5662	277.01	0.97002486
0.00225	1.6533	273.4	0.95738348
0.0034	1.7381	269.34	0.9431663
0.00455	1.8401	266.93	0.93472704
0.00575	1.9239	264.94	0.92775852
0.00695	1.9978	262.91	0.92064993
0.00815	2.1051	260.79	0.91322618
0.0094	2.232	259.35	0.90818363
0.01065	2.346	257.38	0.90128515
0.012	2.5596	253.52	0.88776832

Sample : TS1-200-02
Water condition : Saturated
Particle size distribution : G1
Confinement pressure : 200 (KPa)
Frequency : 2 (Hz)

Gamma [%]	Damping Ratio	G [Mpa]	G/G0
0.00015	2.1156	287.99	1
0.0003	1.7642	284.98	0.98954825
0.00055	1.7607	281.76	0.9783673
0.0009	1.8188	281.75	0.97833258
0.00115	1.8431	279.07	0.9690267
0.0017	1.9625	277.65	0.96409598
0.0023	2.0468	273.76	0.95058856
0.0035	2.1814	269.92	0.93725477
0.00475	2.227	267.15	0.92763638
0.00595	2.3051	265.51	0.92194173
0.0072	2.3856	263.36	0.9144762
0.0085	2.4708	261.76	0.90892045
0.00975	2.5761	260.05	0.90298274
0.01105	2.6878	258.25	0.89673253
0.01245	2.9022	254.99	0.88541269

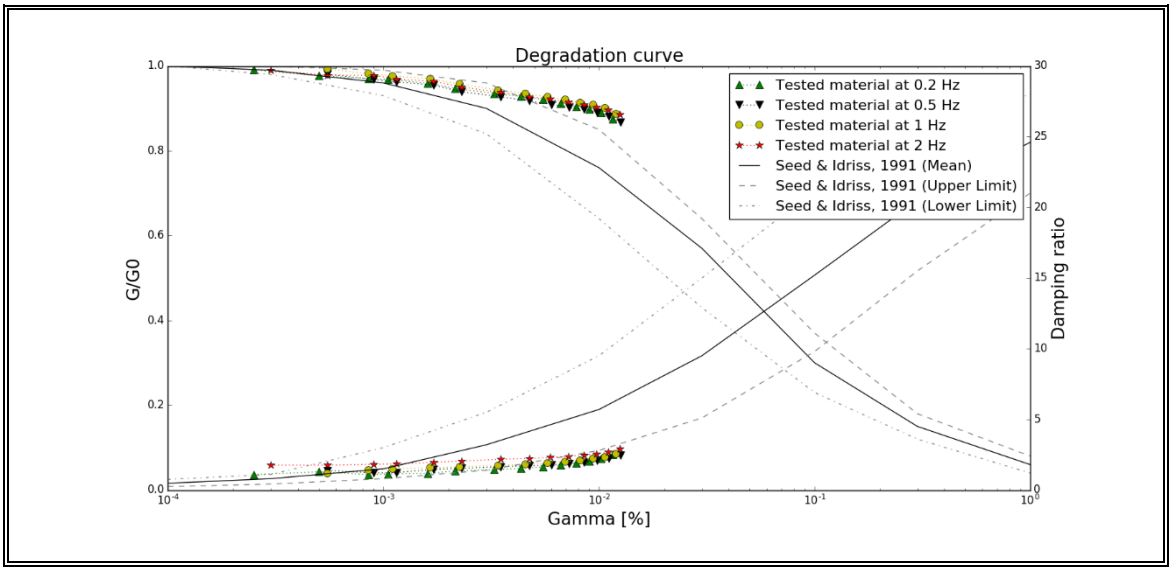

A.5 Cyclic torsional shear test of G2 sample at 100 kPa

Sample : TS2-100-01
Water condition : Saturated
Particle size distribution : G2
Confinement pressure : 100 (KPa)
Frequency : 0.1 (Hz)

Gamma [%]	Damping Ratio	G [Mpa]	G/G0
0.00015	0.2714	154.01	1
0.00025	0.915	151.48	0.9835725
0.0004	0.9708	148.64	0.96513213
0.00085	1.4031	142.99	0.92844621
0.0014	1.6648	138.41	0.89870788
0.00245	2.2911	131.75	0.85546393
0.004	3.5168	122.8	0.79735082
0.0067	6.0633	109.99	0.7141744
0.01	9.0481	98.12	0.63710149
0.0145	12.842	84.8	0.5506136
0.0169	15.5289	76.01	0.49353938
0.02675	19.7787	64.38	0.4180248
0.03505	22.6565	56.18	0.36478151
0.0454	24.8246	48.73	0.31640803
0.0486	25.0629	48.12	0.31244724
0.052	25.4459	47.25	0.30679826

Sample : TS2-100-01
Water condition : Saturated
Particle size distribution : G2
Confinement pressure : 100 (KPa)
Frequency : 0.2 (Hz)

Gamma [%]	Damping Ratio	G [Mpa]	G/G0
0.00005	2.033	160.76	1
0.0001	2.2962	154.4	0.96043792
0.00015	1.5256	156.77	0.97518039
0.0003	1.1694	152.91	0.95116945
0.0005	0.6835	148.72	0.92510575
0.001	1.1473	143.03	0.88971137
0.0017	1.3134	138.49	0.86147052
0.00285	1.7683	132.49	0.8241478
0.00475	2.7286	122.59	0.76256532
0.0078	4.5866	111.58	0.69407813
0.01145	7.0171	101.2	0.62950983
0.01575	9.3486	92.18	0.57340134
0.02145	12.7707	81.11	0.50454093
0.028	15.7167	72.57	0.45141826
0.0353	18.6138	65.75	0.40899478
0.0455	21.3902	57.44	0.35730281
0.05125	22.6786	53.94	0.33553123
0.0656	26.4808	44.22	0.27506843

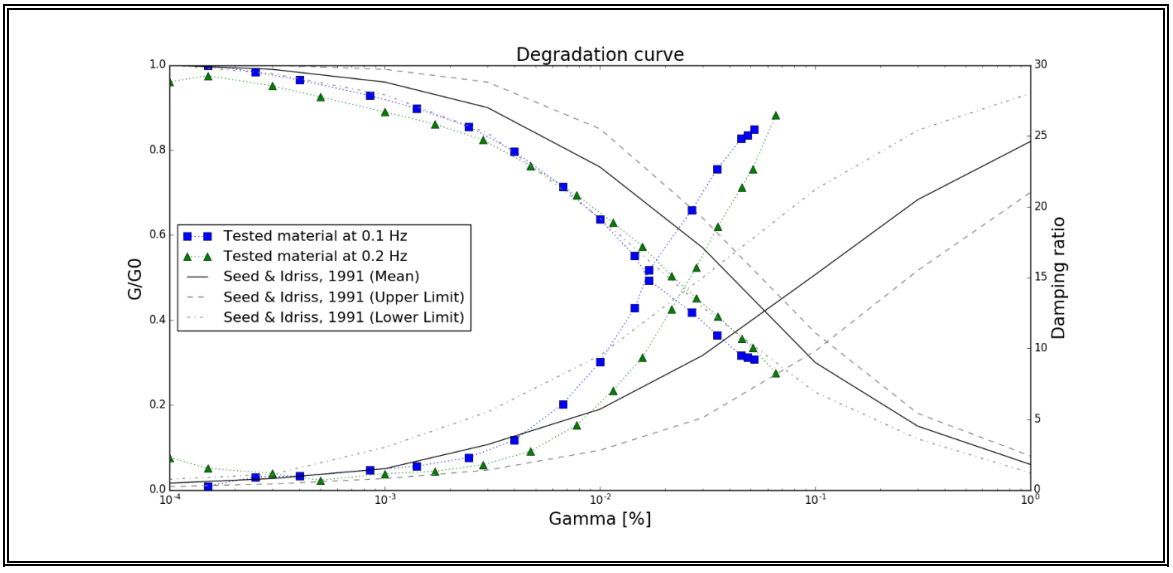

Sample : TS2-100-02
Water condition : Saturated
Particle size distribution : G2
Confinement pressure : 200 (KPa)
Frequency : 0.1 (Hz)

Gamma [%]	Damping Ratio	G [Mpa]	G/G0
0.00005	1.1107	153.39	1
0.00015	1.2431	148.44	0.96772932
0.00025	1.2057	145.97	0.95162657
0.00045	1.0704	144.33	0.94093487
0.00085	1.4308	141.01	0.9192907
0.00145	1.7511	137.48	0.89627746
0.0024	2.3561	132.23	0.86205098
0.00395	3.4917	124.33	0.81054828
0.0065	5.8941	112.98	0.73655388
0.0098	9.0773	100.32	0.65401917
0.01415	13.1129	86.92	0.56666015
0.01995	17.2683	73.97	0.48223483
0.02595	19.6094	66.51	0.43360063
0.0358	23.75	55.11	0.35928027
0.0533	29.1339	42.18	0.27498533
0.0457	24.1775	51.18	0.3336593
0.0632	29.6992	39	0.25425386

Sample : TS2-100-02
Water condition : Saturated
Particle size distribution : G2
Confinement pressure : 200 (KPa)
Frequency : 0.2 (Hz)

Gamma [%]	Damping Ratio	G [Mpa]	G/G0
0.00005	1.4736	160.47	1
0.0001	0.4833	149.95	0.93444258
0.00015	1.1197	148.6	0.92602979
0.0003	0.7712	145.8	0.90858104
0.0005	1.1327	145.5	0.90671154
0.00105	1.2355	141.53	0.88197171
0.0017	1.4338	137.85	0.85903907
0.00285	1.8262	132.79	0.8275067
0.0046	2.6306	125.42	0.78157911
0.00755	4.5367	115.08	0.71714339
0.0111	7.0469	104.36	0.65033963
0.01555	10.2537	93.17	0.58060697
0.0211	13.6	82.44	0.51374089
0.0277	16.5193	73.32	0.45690783
0.03645	19.7772	63.76	0.39733284
0.0475	22.4841	55.03	0.34293014
0.05065	23.0231	54.46	0.33937808
0.0716	28.9644	40.58	0.25288216